Surv. Math. Ind. (1994) 4: 85-149

Surveys on **Mathematics for Industry**

Mathematical modeling in the technology of laser treatments of materials

Vladimir I. Mazhukin and **Alexander A. Samarskii,** Moscow

Summary. In the present review the authors consider the application of mathematical modeling methods for the study of laser radiation influence on absorbing materials. The principle attention is paid to the mathematical formulations of the phenomenon studied as well as the analysis of the simulation results. The numerical solution methods are analysed briefly. It is shown that the mathematical modeling is the main method for theoretical studies of dynamically non-equilibrium phase transformations and processes of plasma formation, which are the basis of numerous kinds of laser treatment of materials.

AMS Subject Classifications: 78A60, 80A22, 35R35.

Keywords: Laser treatment; Stefan problem; Phase transition.

1 Introduction

Rapid development of laser and electron-beam technique has led to the design and implementation of basically new technological processes to solve modern scientific-technical problems mostly arising from the considerably increased requirements about physical-chemical and mechanical properties of materials, the purity and quality of their treatment, as well as the energetic efficiency and safety of technological operations. Concentrated energy fluxes are wide-spread tools for the treatment of metals, dielectrics and semiconductors, meeting in many respects the necessary requirements. At the same time they ensure a high speed performance with excellent degree of precision and location of processes. For this reason such techniques are widely used in metallurgy, mechanical engineering, microelectronics and other branches of modern industry.

More specifically, laser technologies are nowadays an unmatched method for materials treatment. Their characteristics are mostly defined by the features of laser beam as a thermal source. Among their properties it is necessary, first, to underline the high degree of chemical purity as laser influence is a contactless method of energy transfer preventing surface contamination. Laser treatment, as distinct from electron-beam, does not require any vacuum which proves to be a technological advantage in some cases. Lasers with different radiation wavelengths can be used in various processes according to their particular destination. Laser radiation focused into a spot of small diameter can produce the local destruction of practically all materials, allowing the treatment of superstrong and refractory substances. Parallel to the introduction of laser technique, an intensive study on physical-chemical processes in radiated zones is being developed. On one hand, accumulation of knowledge in this dynamic field is necessary in order to acquire fundamental

theoretical notions about the phenomena taking place, as a rule, under conditions of dramatic lack of equilibrium; on the other hand, the study on physical phenomena accomplishing laser radiation influence on the materials is aimed at determining optimum technological process conditions, as well as to improving them and to introducing new methods for treatment.

Modern investigators dispose of three research methods: full-scale experiments, analytical methods, or mathematical modeling. The processes on the whole or their separate elements can be studied by means of full-scale experiments. In the problems of laser action upon condensed media, as a rule, the results for post-action are fixed as some integral effects which often require an additional mathematical solution to be interpreted. The disadvantages of experimental approaches are the limited possibilities for studying processes dynamics, great complication and high cost of equipment. At the same time experimental data are the criterion for validation of any theoretical calculations because in the absence of an experimental validation, the question of their applicability remains open.

Analytical approaches allow to obtain solution in closed form comparatively quickly but generally, they use naive mathematical models requiring strict simplifying assumptions resulting in the idealization of physical processes and simplification of real objects geometry. Thus, the analytical methods often used in engineering calculations make it possible to obtain only some limited information about a strongly idealized picture of physical processes.

Mathematical simulation is an essentially new technology for scientific studies with a number of obvious advantages. Mathematical models to be used for this purpose do not require too strong simplifying assumptions and allow to obtain qualitative and quantitative information about any aspect of a phenomenon. Mathematical simulation may have an essential role in problems describing complex phenomena dynamics. Then it becomes possible to introduce an empirical information into mathematical models and to get numerical experiment essentially close to real physical experiment.

Mathematical modeling becomes an indispensable technique in the field of laser influence on the materials. Most of the applications for laser irradiation are connected with the onset of phase transformations of the first type. Among the mostly used operations of laser treatment we list the following: cutting, drilling, scribing, dimensional treatment, micro remelting, laser deposition, micro welding, as well as welding of large-dimensional parts. All the above technological operations are connected with either melting-crystallization processes or with evaporation or sublimation, or with the whole complex of these processes.

Note that phase transformations of the first type play an essentially important role in technological range of intensities (10^4-19^9 W/cm^2) of laser radiation. However, the state of the total theory of phase transformations does not allow yet to give an answer for certain essential questions even in cases of such evidently well-known processes as melting and evaporation. Active study of phase transformations under pulse influence is in fact only at the beginning and there are still numerous unclear problems and contradictory results. From the point of view of

engineer-technologists, phase transformations are one of the factors finally not understood and essentially influencing the technological processes. Therefore, in order to determine the optimum conditions for laser influence, further additional developments and studies are necessary. Fruitful studies on non-equilibrium phase transformations under laser influence are practically impossible without the help of mathematical modeling allowing to simulate nonlinear situations by means of modern computers, preceding experimental investigations.

The use of powerful personal computers allows to improve the process of mathematical modeling for the experimental devices and technological lines. **In** addition, simulation results can be used directly for further adjustments of technological processes. **In** this connection, the problem of computing automation based on program packages becomes actual.

Note one more important remark. Simulation of laser treatment processes, even in simplified thermodynamical description (namely when hydrodynamical effects are neglected) leads to the consideration of nonlinear problems, whose solution is rather complex. Sometimes this fact is seen as an obstacle to engineering practice. Moreover, the presence of a number of badly controlled parameters such as absorptivity A and spatial fluctuations of intensity G considerably complicates the comparison of calculations with experimental data. Furthermore, the heat transfer problem, as well as Stefan problems occurring in the description of laser heating often do not permit linearization without the loss of accuracy (100-300%) due to the strong dependence on the temperature of physical properties of the conducting material such as surface absorptivity *A(T),* heat capacity *Cp(T),* and thermal conductivity *,1,(T).* As it is known, linear approximations are the basis of engineering calculations, but in the field we are considering, they have to provide an accuracy within 5-10%. Therefore, most of the problems for laser heat are solved empirically and absorptivity *A(T),* for example, is used as an adjusting parameter. Nevertheless, the amount of papers showing rather good agreement of calculations with experiments is very small. This is due on one hand to the not too high accuracy of experimental description of such parameters as condensed phase temperature, and on the other hand to the absence of reliable comparison procedures. As a rule, comparison of calculated data with experimental ones is made by melting isotherms [1]. Therefore, systematic comparison of calculated values of temperature with experimental ones for various materials is not available even when phase transformations do not occur.

In our opinion, the application of traditional engineering computing schemes in the laser technology problems is not suitable. **In** theoretical studies for the effect of concentrated energy fluxes upon a material it is necessary to use the essentially nonlinear mathematical models realized as compact highly efficient program packages oriented for personal computers. Such physical quantities as Cp(T),).(T), *A(T)* are defined either experimentally or from theoretical studies, including computing experiment. The methods for the numerical solution of differential problems which we are developing and using are based on the classical concepts of computing mathematics: conservativity, homogeneity, and adaptivity [2] which guarantee high computing efficiency.

Mathematical modeling and computing experiments are successfully used to study and predict the solutions to many complex problems of physics and technology. The present paper deals with the review of the most important and interesting problems of laser technology, the solution of which requires a wide application of mathematical modeling. Visualization of these problems is based on longterm experience of the authors' work in this field.

The paper is organized as follows. In Sect. 2 we discuss the applicability of numerical experiments to the laser thermo hardening problem. Computational results are provided for three-space-dimensional temperature field in steel plate heated under the influence of a moving energy source. Values of influence parameters were assumed to be typical for laser technology.

In the other sections the principal attention is paid to the phase transition dynamics and first of all to the melting and evaporation problems, that provide the basis of many laser technologies. In Sect. 3 we provide a brief classification of physical mathematical formulations for phase transition problems, deduced from several variations of the Stefan problem. We also analyze the main numerical methods for solving such problems. Particularly we consider the solution of two-space-dimensional enthalpy-formulated crystallization problem for metals. The main attention is paid to dynamic adaptation method, proposed by authors. Numerically examined by means of this method are some problems, typical for pulse laser influence. The application of dynamic adaptation method allows direct phase front tracking and the determination of such important technological parameters as the front propagation velocity, the melted and evaporated layers depth and the pressure on the evaporation boundary along with the temperature field in the material. The method also enables the analysis of such an insufficiently investigated phenomenon as overheated metastable states formation in condensed media.

Section 4 is devoted to the modeling of melting and evaporation processes in homogeneous materials, providing the basis of such technological operations as laser treatment of coating, plating and surface modification of metals. As an example, melting, crystallization and evaporation processes in two-layer Ti-AI plate are numerically analyzed by means of dynamic adaptation method.

Section 5 is devoted to the evaporation kinetics analysis under wide range of parameters. The mathematical models considered describe metal evaporation into vacuum for two essentially different regimes: with or without plasma formation in the evaporated substance. The consideration of these processes inevitably leads to a system of coupled equations: the heat equation for the condensed medium and the radiational gas-dynamics equations for the evaporated substance. As mathematical modeling showed the nonequilibrium degree for liquid-vapor phase transition and consequently a value of mass flow across the interface in some cases are determined not only by temperature regimes (thermodynamical factor), but by gaseous media behavior (gas-dynamic factor) as well.

In Sect. 6 a problem for optical breakdown in aluminum vapor is formulated on the basis of collisional-radiational transitions analysis. The mathematical model provides a coupled system of chemical kinetics equations and two energy equations. The essentially nonequilibrium regime was determined for electron

avalanche formation and threshold values of energy source necessary for breakdown were found. The gas-dynamic stage of laser plasma formation is examined on the basis of the two-space-dimensional radiational gas-dynamics model. The main mechanisms of propagation of plasma formations are analyzed by means of mathematical modeling and an optimal regime for laser-plasma treatment is proposed.

In Sect. 7 we consider the main characteristics of LASTEC-S program packages developed by the authors for automatic computation of laser influence.

2 Laser thermohardening

It is known [1, 3] that laser radiation with intensity $G \leq 10^6$ W/cm^2 upon strongly absorbing condensed media is equivalent to the influence of a thermal source of the corresponding power. Laser heating of solids without melting and evaporation of the heated surface is generally referred to as thermal treatment. Its main objective is the change of microhardness and finally, of wear resistance of the material to be treated. Laser surface treatment of ferrous metals and their alloys are nowadays one of the most important fields of application of laser technology. Its principal advantages with respect to traditional methods for hardening, for example, induction or contact with gas-flames, consist in increasing productivity and quality, energy efficiency due to selective treatment of separate areas, the possibility of using cheap raw materials, improving their mechanical quality, and the possibility of treating complex geometries with simultaneous strain reduction. Laser hardening is mostly used in technological lines of engineering industry. For its realization, laser devices working in pulse mode or in continuous mode under scanning condition are used.

Surface thermohardening is connected with the increase of microhardness of a material in the region of influence which is obtained by rapid heating of thin, 0.1–1 mm, near-surface layer by laser radiation with simultaneous cooling due to heat transfer to substrate. The underlying physical mechanism includes phase transformation and structural changes related to the formation of various non-equilibrium states, to the milling of original metal grains into smaller blocks and to the generation of a large amount of dislocations under the influence of rapid temperature changes and strong thermal strains.

Generally, the thermal cycle of surface hardening for ferrous metals consists of two stages: heating and cooling. For example, surface hardening of steels is based on different solubility of doping impurities and carbon in high-temperature (γ-phase) and low-temperature (α-phase) forms of iron. During the first stage of thermohardening, heating up to temperatures above the temperature of the $\alpha \rightarrow \gamma$ transition (phase transition of the first type) but below the melting temperature can lead to the complete dissolution of carbon. Solid solution of carbon in γ-phase is called austenite. During the second stage of thermohardening, high speed cooling, the process runs in the reverse direction ($\gamma \rightarrow \alpha$ transition). Carbon excess produced by $\gamma \rightarrow \alpha$ transition is usually extracted as ferric carbide. However, under very rapid cooling, order of 10^8 K/s, typical for the process discussed, carbon has no time to be extracted, thus giving rise to the formation of a non-equilibrium state called martensite. Such a phenomenon is accompanied by the appearance of a large

amount of new surfaces preventing dislocation motion, which along with oversaturated solution of carbon, leads to microhardness increase.

The kinetics of martensite-austenite transitions is still insufficiently studied but at present it is the object of intensive investigations [4–6]. Therefore, in practice, in order to optimize the conditions for surface hardening, the trend is to obtain reliable information on temperature fields dynamics and to use it for correction of the technological process. When studying metals heating by laser radiation it is important to know the process characteristics: spatial distribution of temperature fields, their gradients, heating and cooling velocities, as well as the thermal influence zone.

As a typical example, a laser heating problem was considered for a solid with normal incident laser beam moving along the y-axis at speed v (Fig. 1). It is suggested, that laser radiation is volumetrically absorbed by the material according to the exponential law.

$$G(x, y - vt, z) = G_f(x, y - vt) \exp\left(- \int_0^z \kappa dz \right), \quad 0 < z < l_3$$

where $G_f(x, y - vt)$ is the radiation intensity in the focal plane and κ is the absorption coefficient.

To describe the heating process we consider a boundary value problem for heat and radiation transfer equations.

$$\rho C_p(T) \frac{\partial T}{\partial t} = \operatorname{div} \lambda(T) \operatorname{grad} T - \frac{\partial G}{\partial z}, \tag{2.1}$$

$$\frac{\partial G}{\partial z} + \kappa G = 0, \tag{2.2}$$

$$0 < x < l_1, \quad 0 < y < l_2, \quad 0 < z < l_3.$$

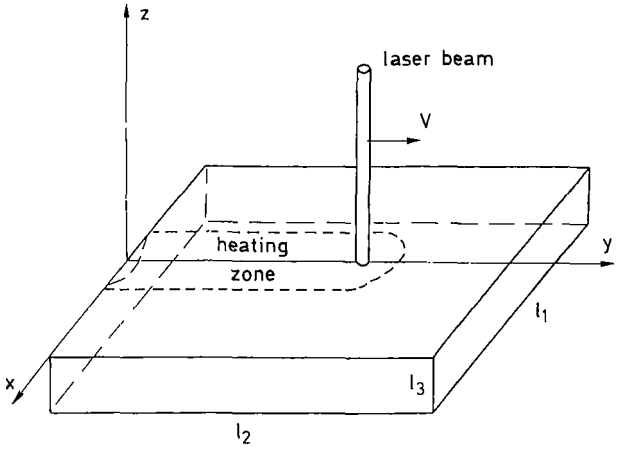

Fig. 1

The plate boundaries were considered to be heat impermeable, i.e., the heat transfer equation (2.1) was supplemented with boundary conditions of the second type. It was also supposed that G_f could be described by the normal distribution law:

$$G_f(x, y - vt) = G_0 \exp[-(x^2 + (y - vt)^2)/2R^2] \tag{2.3}$$

where $G_0 = P/(\pi \cdot R^2)$ represents the intensity in the focusing spot center, P is the radiation power, and R is the radius of the focusing spot. The boundary condition for the radiation transfer equation (2.2) was formulated on $z = 0$, taking into account the absorptivity $A(T)$ of the radiated surface:

$$G(x, y - vt, 0) = A(T)\, G_0 \exp[-(x^2 + (y - vt)^2)/2R^2]. \tag{2.4}$$

In general $A(T)$ depends on the material, on the surface quality, on the angle of incidence and on the surface temperature as well.

The nonlinear problem (2.1)–(2.4) was numerically solved by finite difference method [2]. As a material, steel was chosen letting its thermodynamical parameters vary within the temperature range $T_0 < T_{max} < T_m$ as follows:

$$0.48 \leq \lambda \leq 0.23 \text{ W/(cm K)}, \quad 0.35 \leq C_p \leq 0.5 \text{ J/(g K)}.$$

Radiation intensity G_0 and laser beam velocity v were varied within the ranges: $10^4 \leq G_0 \leq 10^5$ W/cm^2 with $\lambda = 10.6$ μm and $2.5 \leq v \leq 25$ m/s. The absorptivity of surface in the given intensity range was considered to be little dependent on temperature and in calculations was prescribed as constant $A = 0.1 - 0.2$.

In Fig. 2 typical spatial profiles for temperature fields on various material depths are given. The conditions were chosen in such a manner that the maximum temperature T_{max} on the surface is consistent with the bounds $T_0 \leq T_{max} \leq T_m$. The total view of curves shows that the temperature fields created in the material by the movable source are non-symmetric. Increase of intensity and laser beam velocity induces, on one hand, an increase of heating and cooling speeds necessary for hardening, and on the other hand, leads to a higher torsion of fronts characterized by steep gradients. The appearance of high gradients is accompanied by strong thermal strains which can eventually lead to a decreasing of microhardness. According to the given figures, the highest gradients arise at the top surface and in a thin layer underneath, especially, on the boundaries of thermal influence zone. Thus, the knowledge of the temperature evolution allows to establish necessary thermal cycles resulting in the required changes of microstructure in the zone of influence.

Note that the main problems of mathematical modeling in the field of laser technology are related to the insufficient development of the theoretical description of the kinetics of phase transformations of the first type. Some difficulties arise also with numerical solution of problems with complex geometrical shape.

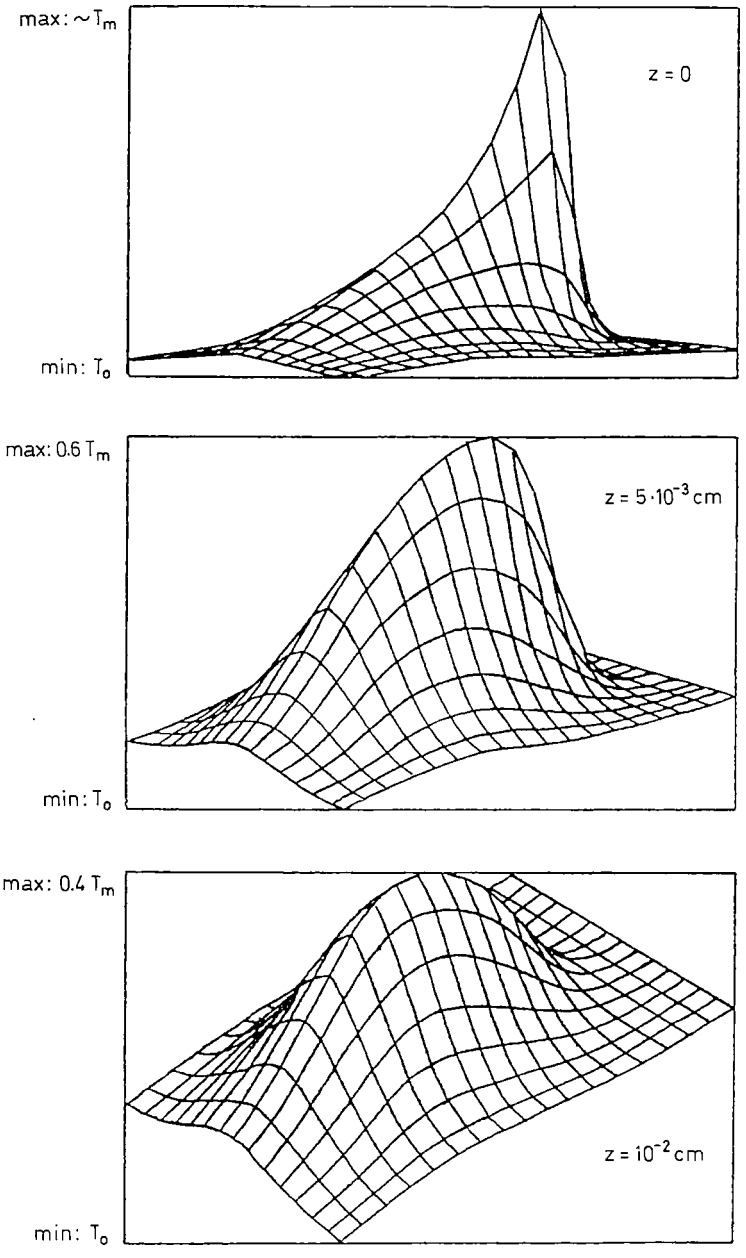
max: ~T_m
z = 0
min: T_0
max: 0.6 T_m
z = $5 \cdot 10^{-3}$ cm
min: T_0
max: 0.4 T_m
z = 10^{-2} cm
min: T_0

Fig. 2

3 Laser treatment based on phase transformations The main mathematical models and methods for their solution

The great majority of applications of laser effect upon materials is connected with the onset of phase transformations of the first type: melting, evaporation, crystallization and condensation.

Phase transformations of the first type play an important role within the whole technological range of laser radiation intensities, however, the state of the general theory of phase transformations does not allow yet to give answers to some essential questions, even in the case of such widely known transformations as melting and evaporation [7].

The problem of the theory of non-equilibrium phase transformations, reflects to a certain extent the difficulties which arise when describing strongly non-equilibrium processes in macroscopic systems.

The absence of phase equilibrium is a necessary condition for phase transformation. The dynamics of non-equilibrium phase transformations depends in a sensitive way on how deeply the process considered comes into the metastable states region. High heating and cooling rates to be realized under intensive laser pulses lead deeply into the metastable states region. Rapid cooling due to high temperature gradients under pulse influence is used to obtain "frozen" metastable states with qualitatively new properties. In particular, metastable states are the basis for obtaining amorphous metal alloys and semiconductors differing from the materials with crystal structure by higher strength and corrosion resistance.

In fact, an active study of phase transformations under pulse influence is only at the beginning and in this area there are still many unclear problems and contradictory results. No progress on the problem of non-equilibrium phase transformations with laser influence on condensed media is practically possible without the help of mathematical modeling.

Theoretical investigation for dynamics of the first type phase transitions leads to different variations of the Stefan problem [8], under which heading a very large class of free boundary problems for parabolic or elliptic equations are collected. A quite general formulation of the Stefan problem consists in a boundary value problem for a quasilinear parabolic equation with piecewise-continuous coefficients, having discontinuities on level sets of the unknown function.

There is a very large number of publications devoted to the Stefan problem, in view of the relevant scientific and practical interest of phase transitions and its various technical applications. Theoretical papers can be classified into several groups in various ways. One group, devoted to the mathematical structure and to the qualitative properties of solutions, deals with existence and uniqueness theorems for classical or generalized solutions. Many papers [9–18], reviews [19–24], and monographs [25–28] are devoted to this subject. Another group is connected with the development of numerical methods and with their applications. Too, there is a variety of papers in this especially fast developing field [29–49]. Thus a full review of the Stefan problem should be the subject of individual consideration, as well as exhaustive bibliography of this problem.

The classification above is not rigid and is introduced just for the sake of conciseness. In the sequel we only deal with the methods more frequently used in mathematical modeling for this problem. So that one should not consider this section as an attempt to review the literature concerning the Stefan problem. This paper covers only some aspects of this general problem directly connected with mathematical modeling of laser influence.

3.1 Classic version of Stefan problem Melting-crystallization

Let us write down the most commonly used mathematical models for Stefan problem referring mainly to one-space-dimensional formulations. The analysis of these models allows, on one hand, to establish the main physical objective laws of the processes and, on the other hand, to determine the characteristic peculiarities of different methods for the numerical solution of multi-dimensional problems.

The classic version of the Stefan problem formulated around the end of the last century for phase transformations, melting or crystallization type, contains first of all the heat transfer equation in the region with a priori unknown moving boundary which separates solid s and liquid l phases:

$$\left[\rho C_{\mathrm{p}} \frac{\partial T}{\partial t} = \frac{\partial}{\partial x}\left(\lambda \frac{\partial T}{\partial x}\right) + Q\right]_k, \quad k = s,l, \tag{3.1}$$

where $\rho_k \cdot C_{\mathrm{p}}$ is the volumetric heat capacity, λ is the thermal conductivity and Q_k is the volumetric power of heat sources. At phase interface a so-called Stefan condition is fulfilled,

$$\lambda_{\mathrm{s}} \frac{\partial T_{\mathrm{s}}}{\partial x} - \lambda_l \frac{\partial T_l}{\partial x} = \rho_s L_m v_{sl}. \tag{3.2}$$

The physical interpretation of the Stefan condition is the following: the interface velocity, v_{sl}, is defined by heat flux absorbed or extracted on this boundary due to volumetric heat of phase transformation, $\rho_s \cdot L_m$. Relations (3.1)–(3.2) for simplicity are written in the one-space-dimensional case with a planar interface.

Besides the free boundary condition (3.2), one more condition connected with phase transformation kinetics is necessary. In melting or crystallization problems it is usually assumed that on the interface, the temperature is continuous and equal to the equilibrium transition temperature, denoted T_m:

$$T_{sl} = T_s = T_l = T_m. \tag{3.3}$$

T_m in many cases can be considered as a constant value. Variation of T_m may result from change of outer pressure or variation of substance properties occurring at the transformation front.

It must be noted that nonequilibrium states occurring in phase change processes are not included in the classical Stefan problem [8]. Such an approach and its various modifications are widely used to describe phase transformations with pulse influence of concentrated energy fluxes [50] and undoubtedly it has a certain

range of application. However, the question of its applicability in some practically important cases remains still open. The assumption of constant temperature on the phase boundary proves to be correct, for example, for solid-liquid transformations with relatively low radiation intensities in which temperature changes are slow.

Problems like (3.1)–(3.3) complemented by appropriate boundary and initial conditions are non linear even at constant values of thermodynamic parameters, therefore, their analytic solution can be determined only for some special cases. The main difficulties with numerical solution of such problems are related to the presence of moving boundaries.

3.2 Enthalpy formulation

Widely used in theoretical investigations and in the numerical analysis is another principal approach, known as enthalpy formulation. The enthalpy approach is based on bypassing the direct search of interface location, solving instead a nonlinear heat transfer problem, written in the whole domain. To provide such formulation, the coefficients smoothing technique is used, proposed in [9, 10] in the theory of quasilinear parabolic equations for generalized solution construction. An effective heat capacity concept is introduced for the heat equation, including the latent heat of phase transition by means of Dirac type singularity at the interface. In this way the problem is summarized by the following quasilinear heat transfer equation:

$$\rho C_p \left(1 + \frac{L_m}{C_p}\delta(T - T_m)\right)\frac{\partial T}{\partial t} = \frac{\partial}{\partial x}\left[\lambda \frac{\partial T}{\partial x}\right] \tag{3.4}$$

to be solved in the entire domain with appropriate initial and boundary conditions. The boundary condition for the interface (Stefan condition (3.2)) is not explicitly used in this formulation of the problem, but it can be derived from Eq. (3.4).

Note that the homogeneity principle for differential equations and for corresponding numerical methods is used not only in the Stefan-problem framework, but has also a great importance in mathematical modeling of different processes, described by p.d.e's. We refer for instance to the homogeneous computation method of discontinuous flows in gas dynamics, based on smoothing of jump discontinuities by artificial viscosity [51, 52].

3.3 Non-equilibrium version of Stefan problem

More generally, the description of dynamics of rapid phase transformations, typically accompanying high power laser radiation, can be done with a phenomenological condition different from (3.3). Proceeding from the general theory for phase transformation kinetics, it is possible to write down the condition connecting

the velocity of phase interface, v_{sl}, with the interface temperature, T_{sl} [53]:

$$v_{sl}(T_{sl}) = C \exp\left[\frac{A}{RT_{sl}}\right]\left[1 - \exp\left(\frac{\Delta G}{RT_{sl}}\right)\right] \tag{3.5}$$

where C is a constant, A is the activation energy, ΔG represents the change of free energy, R is the ideal gas constant. In the engineering applications this approach is not of frequent use and so far it was mainly adopted to describe crystallization processes [54, 55].

3.4 One-phase version of Stefan problem Evaporation

Evaporation is the process of the transformation of a substance from condensed to gaseous state and it is characterized by high energy capacity and specific volume if compared with melting. Laser evaporation of metals can proceed in two essentially different modes if the temperature and pressure values lie in the subcritical region and the liquid–vapor interface is well-defined. In the first mode the evaporation velocity is equal to velocity of sound. This is a typical situation for evaporation to vacuum or to media with negligible pressure as compared to the pressure of saturated vapor. In this case gas-dynamic disturbances in evaporated substance flux have no effect upon the behavior of condensed medium and the description of the processes is considerably simplified [56] as the problems in the condensed and in the gaseous phase seem to be independent of each other and they can be considered separately. In the second mode, typical for evaporation into medium with counter-pressure, the evaporation velocity can be lower than the sound velocity and so gas-dynamics can play a determining role in the behavior of the overall process [57]. In this case, the problem is considerably complicated because the processes in condensed and gaseous phases appear to be interrelated. First, we consider the mathematical model for evaporation when the evaporation velocity is assumed to be equal to sound velocity.

To describe the process for surface evaporation, it is usual to exploit the version of Stefan problem [58] in which flat front transition temperature depends weakly (logarithmically) on the front velocity, v_{lv}. Three conservation laws (for mass, momentum, and energy) are written down on the phase interface Γ_{lv}:

$$\begin{aligned} \rho_l v_{lv} &= \rho_v (v_{lv} - u), \\ \mathrm{P}_l + \rho_l v_{lv}^2 &= P_v + \rho_v (v_{lv} - u)^2, \\ -\lambda_l \frac{\partial T_l}{\partial x} &= G_l - \rho_l L_v v_{lv} \end{aligned} \tag{3.6}$$

where the index v denotes vapor, G_l is energy source intensity, u is hydrodynamical velocity of vapor, P is pressure. We also write down two additional relations describing the kinetics of phase transformation and the degree of non-equilibrium

for the overall evaporation process. In the Knudsen layer approximation [56] these relations take the following form [59]:

$$T_v = T_l \cdot \left\{ \left[1 + f^2 \cdot \left(\frac{\gamma - 1}{\gamma + 1} \right) \cdot \mathrm{M}^2 \right]^{1/2} - f \cdot \left(\frac{\gamma - 1}{\gamma + 1} \right) \cdot \mathrm{M} \right\}^2$$

$$\rho_v = \frac{1}{2} \rho_H \left\{ \left(\frac{T_l}{T_v} \right)^{1/2} \cdot \left[(\gamma \mathrm{M}^2 + 1) \exp(b^2 \mathrm{M}^2) \operatorname{erfc}(b\mathrm{M}) - \frac{4f}{\pi} \mathrm{M} \right] \right.$$

$$\left. + \frac{T_l}{T_v} \left[1 - 2 \cdot f \cdot \mathrm{M} \exp(b^2 \mathrm{M}^2) \operatorname{erfc}(b\mathrm{M}) \right] \right\} \tag{3.7}$$

$$b = (\gamma/2)^{1/2}, \; f = \left(\frac{\pi\gamma}{8} \right)^{1/2}, \; \mathrm{M} = \frac{u}{u_c}, \; u_c = (\gamma R T_v)^{1/2},$$

where u_c is the sound velocity and ρ_H denotes the saturated vapor density.

3.5 Hydrodynamical version of Stefan problem

One-space-dimensional hydrodynamical model of Stefan problem can be applied to describe photoacoustic effects arising in condensed media under the influence of pulse radiation [50], as well as to consider the influence of equilibrium phase transformation temperature dependence on pressure, $T_m = T_m(P)$, during melting process. The corresponding mathematical model is as follows:

$$\left[\frac{\partial \rho}{\partial t} + \frac{\partial}{\partial x} (\rho \cdot u) = 0 \right]_K,$$

$$\left[\frac{\partial}{\partial t} (\rho \cdot u) + \frac{\partial}{\partial x} (\rho \cdot u^2) = - \frac{\partial p}{\partial x} \right]_K, \tag{3.8}$$

$$\left[\frac{\partial}{\partial t} \left[\rho \cdot \left(\varepsilon + \frac{u^2}{2} \right) \right] + \frac{\partial}{\partial x} \left[\rho \cdot u \cdot \left(\varepsilon + \frac{u^2}{2} \right) \right] = - \frac{\partial}{\partial x} (p \cdot u) + \frac{\partial}{\partial x} \lambda(T) \cdot \frac{\partial T}{\partial x} \right]_K,$$

$$K = s.l;$$

$$x_0 < x < \Gamma_{sl},$$
$$\Gamma_{sl} < x < x_N.$$

The symbols ρ, u, p represent density, hydrodynamic velocity and pressure respectively, while λ denotes thermal conductivity and ε the internal energy. The given system is supplemented with the appropriate state equations:

$$[\varepsilon = \varepsilon(\rho, T)]_K, \quad [p = p(\rho, T)]_K.$$

and boundary conditions. On phase interface the relations for one of the versions of Stefan problem (equilibrium, nonequilibrium) has to be considered.

3.6 Methods for numerical solution

Due to the presence of moving phase boundaries, the Stefan problem is nonlinear, even with constant thermodynamical and optical parameters. Non-linearity of the problem makes it difficult to emphasize the main features of heat model and to obtain analytical solutions. In general case, the determination of temperature profile in a Stefan problem is possible only by means of numerical methods.

The methods presently available for numerical solution of Stefan problems can be conventionally divided into two broad classes: methods with explicit front-tracking and smoothing methods. Numerical methods including the procedure of explicit phase fronts tracking are remarkable for the great variety of approaches. Among them the most widely used are: method for front trapping into a node [31] in which by means of an iteration procedure, the integration time step is chosen in such a way that phase boundary is shifted one interval in space; method of straight lines [32, 33]; method of straightened fronts [34] based on the substitution of spatial variable with transformation $x = \xi \cdot \eta$, where ξ characterizes the phase boundary position; methods for isotherms migration [36] in which dependent and independent variables are exchanged. As a rule, these methods have sufficiently high precision of front tracking but become algorithmically rather bulky and require high expenditures of computer time in case of multi-phase and multi-dimensional problems.

3.7 Smoothing methods

The absence of sufficiently effective algorithms for numerical solution of classic Stefan problem and increasing number of applied problems stimulated the development of another approach to numerical solution of Stefan problem. For mathematical modeling of a certain class of problems connected with phase transformations where precise interface position does not play an essential role, the methods using the technique of enthalpy smoothing proved to be effective. Numerical methods based on this approach work over the whole region considered, recovering the location of the phase boundary in a fully implicit way [30, 37]. The efficiency of these algorithms is especially noticeable in multi-dimensional problems [30, 37–39]. The disadvantages of the smoothing methods usually consist in low precision of front tracking and their sensitivity to the choice of the smoothing parameter [40], whose optimal value is difficult to be determined a priori.

As an example of application of the given algorithm, consider the problem of crystallization of liquid metal subject to a cooling flux [40]. The problem is formulated as follows. A cooling flux, q, acts on the surface of rectangular metal melt-filled bath with heat-impermeable walls. At time $t = 0$ the melt has the temperature equal to the melting temperature, T_m. It is necessary to determine the dynamics of the crystallization front advancing from the surface into the melt and the spatial-time temperature distribution corresponding to various spatial profiles of cooling flux, $q(x)$. From the mathematical point of view, the problem leads

to the integration of a non-stationary heat transfer equation in a rectangle, $\Omega(x, y) \in [0, l_1] \times [0, l_2]$, with boundary conditions of the second type:

$$\frac{\partial H}{\partial t} + \operatorname{div} \vec{W} = 0, \quad \vec{W} = -\lambda(T) \operatorname{grad} T,$$

$$H = [\rho C_p + L_m \cdot v(T - T_m)] \cdot T, \quad (x, y) \in \Omega, \quad t > 0,$$

$$v(T - T_m) = \begin{cases} 1, & T > T_m \\ 0, & T < T_m \end{cases}, \tag{3.9}$$

$$y = 0: \quad -\lambda \frac{\partial T}{\partial y} = q(x), \quad x = 0: \quad -\lambda \frac{\partial T}{\partial x} = 0,$$

$$y = l_2: \quad T = T_m, \quad x = l_1: \quad -\lambda \frac{\partial T}{\partial x} = 0,$$

$$t = 0: \quad T(0, x) = T_m.$$

For ρ, $C_p(T)$, $\lambda(T)$, the values typical for zinc have been chosen. l_1 and l_2 are given as equal to 10 cm and 5 cm, respectively.

In finite differences approximation of (3.9) the discontinuous function $v(T - T_m)$ has been replaced by a continuous function $v_\Delta(T)$. Two different approximations have been considered, differing from each other by their smoothness degree.

A typical approximation is the linear one [30, 41, 42]:

$$v_\Delta(T) = \begin{cases} 1, & T \geq T_{\max} \\ (T - T_{\min})/\Delta, & T \in (T_{\min}, T_{\max}) \\ 0, & T < T_{\min} \end{cases} \tag{3.10}$$

where $\Delta = (T_{\max} - T_{\min}) > 0$ is a parameter, defining the width of jump smoothing. Also the exponential function approximation has been used, [40]:

$$v_\Delta(T) = 1 - [1 + \exp\{4 \cdot (T - T_0)/\Delta\}]^{-1}, \tag{3.11}$$

where T_0 is the inflection point of $v_\Delta(T)$.

In the first case, the smoothing interval is finite and equal to Δ and in its extreme points, $T_{\max}$ and $T_{\min}$, the derivative of the function v_Δ has discontinuity of the first type. In the second case, the smoothing interval is infinite but it is possible to emphasize an effective interval of smoothing Δ: $(T - \Delta/2, T + \Delta/2)$. Function $v_\Delta(T)$ is C^∞.

The influence of the approximation of v on the solution was studied on two problems with sinusoidal and exponential spatial distribution of source $g(x)$:

$$g(x) = g_0\left(1 + A \sin \frac{2\pi x}{L_x}\right), \; g_0 = 10 \text{ W/cm}^2, \; A = 0.2,$$

$$g(x) = g_0 \exp\left\{-\frac{(x - m)^2}{k}\right\}, \; g_0 = 21 \text{ W/cm}^2, \; m = \frac{1}{2}x, \; k = 3.48.$$

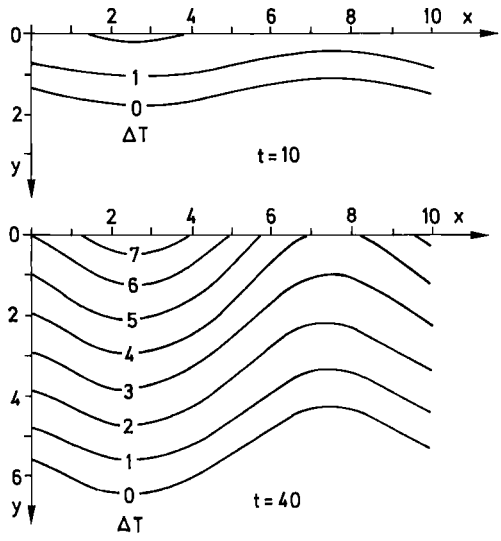

Fig. 3

Note that numerical integration of boundary value problem with boundary conditions of the second type is studied to a lesser extent and for such problems an additional requirement exists for Δ to be as small as possible.

The distribution of temperature fields and position of phase boundary $\Delta T = 0$ for both sources at different time instants are given in Figs. 3 and 4. Isotherms in Figs. 3 and 4 are shown in relation to temperature T_m, $\Delta T = T_m - T$. The zero isotherm, $\Delta T = 0$, corresponds to phase boundary. For the linear approximation of $v(T - T_m)$ an 8 times decrease of the smoothing parameter Δ (i.e., 1°) requires the reduction of the integration step Δt approximately by two orders. While for the exponential approximation of $v(T - T_m)$ a 100 times decrease of Δ practically has no influence on the integration step.

However, it is necessary to note that the smoothing procedure of the enthalpy function applies to a restricted class of problems, excluding in particular the processes of overheating or overcooling of a condensed medium. In the latter cases when physical conditions permit the appearance of overheated or overcooled states, the use of such an approach can lead to the failure of the definition of temperature field and phase boundary velocity. Additional limitations arise in connection with correct statement of boundary conditions in cases when the complete system of hydrodynamic equations is used to describe the process [43–46].

3.8 Dynamic adaptation methods

Numerical algorithms based on the methods of dynamic adaptation of computational grids for the solution specially developed for Stefan problems [60, 61] and allowing to analyze both one- and multi-space-dimensionally all problems are free of the disadvantages discussed above [62]. In the dynamic adaptation methods the problem of constructing the computational grid is formulated at differential level.

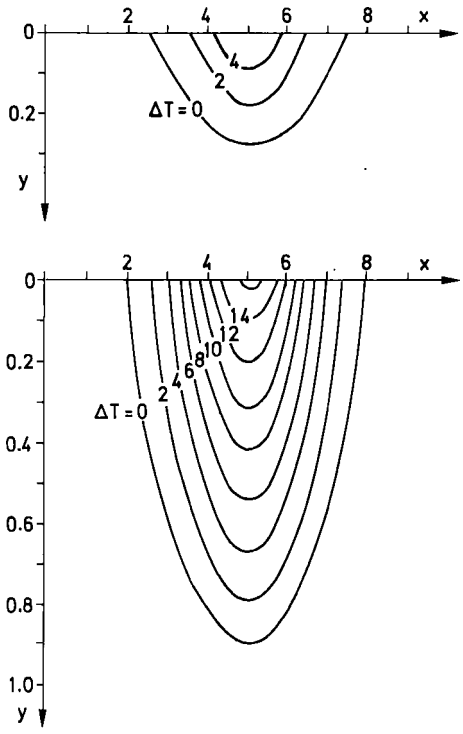

Fig. 4

In the differential problem some equations describe physical processes and the others the behavior of grid points [63].

The main source of complexity for the numerical solution of Stefan problems is the presence of unknown moving boundaries. The dynamic adaptation method is based on the automatic transformation to a moving coordinate system driven by the solution to be determined. The transition to moving coordinates system allows to eliminate the problems related to moving boundaries but in this case it is necessary to determine not only the values of unknown functions but also the grid points coordinates. The description of the grid points movement is performed by partial differential equations added to the problem. The number of such equations is equal to the space-dimensionality of the problem. The adaptation mechanism of computational grids in the proposed method is introduced at differential level and does not depend on the specific numerical method employed (finite differences or finite elements). The behavior of additional equations considerably depends on the dynamics of the physical process. The transformation of coordinates driven by the solution itself allows to dislocate grid points depending on particular features of the solution such as the spread of large gradients, shock waves, contact and phase boundaries. The density of points in the regions of fast changing solution in the dynamic adaptation methods is determined with the help of a transformation function, Q, which generally can be the combination of the solution and of its derivatives [64, 65].

As it was already noticed, the problems connected with moving boundaries are eliminated by passing to a moving coordinate system in which grid points and boundaries are fixed. In this respect the method is similar to Lagrangian methods. However, there is a principal difference. In Lagrangian methods for moving coordinates system the hydrodynamical velocity is increased: this is not always convenient and considerably restricts the class of solvable problems. In the dynamic adaptation methods the velocity of coordinates system (and respectively, the grid points distribution) is not indicated a priori and is determined in the process of solving of the problem. It principally allows to obtain any desired points distribution and the application of the method is not limited by the problems of hydro- and gas-dynamics. For the complete description of the principles for constructing dynamically adapting algorithms for free boundary value problems we refer to [65].

In conclusion, we note that during the last years most attention has been given to the problem of computational grid generation, being of paramount importance in numerical solutions of mathematical physics equations. Several general directions to grid generation and adaptation can be found in the literature [66–78]. Nevertheless the methods of adaptive grid generation are developing intensively and at present it is impossible to say which ones are preferable.

The efficiency of the dynamic adaptation method is shown in the following two tests which refer to essentially different problems. The first problem deals with laser melting and evaporation of condensed media [79]. The mathematical model describing these processes represents the classic one-phase Stefan problem. In the second problem, associated with the Stefan hydrodynamical model, we consider metal melting from an overheated initial state [80].

3.9 The problem of laser melting and evaporation [79]

In Fig. 5, laser radiation is spread along the axis x from right to left. In points $x = \Gamma_{sl}$ and $x = \Gamma_{lv}$ and $x = \Gamma_{lv}$ solid–liquid and condensed medium–vapor interfaces are located.

At the body surface, laser flux is partially absorbed producing heating, melting or evaporation depending on the intensity and duration of the pulse influence.

Surface and volumetric energy absorption

During heating the volumetric and surface energy absorption of electromagnetic radiation is distinguished depending on correlations between absorption coefficient values κ and thermal influence length $l_T = (a \cdot t)^{1/2}$. If the latter is much

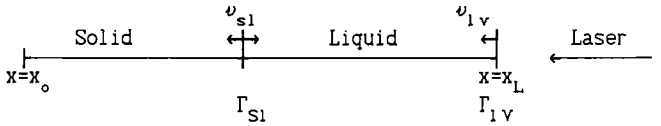

Fig. 5

higher than the mean photon free path $l_p = \kappa^{-1}$ ($l_T \gg l_p$), the conversion of radiation into thermal energy occurs entirely at the surface. In the opposite case, ($l_T \leq l_p$) energy penetrates and is absorbed volumetrically. Volumetric heating by laser radiation can produce phase transformation if $\kappa \cdot a/V_{sl} \leq 1$, i.e., if energy absorption length is not small as compared with thermal influence length.

The volumetric absorption of laser radiation is described by the energy balance equation and the radiation transfer equation:

$$C_p(T)\,\rho(T)\frac{\partial T}{\partial t} = \frac{\partial}{\partial x}\lambda(T)\frac{\partial T}{\partial x} - \frac{\partial G}{\partial x}, \tag{3.12}$$

$$\frac{\partial G}{\partial x} + \kappa G = 0. \tag{3.13}$$

On the surface to be irradiated, $x = x_L$, the following boundary conditions are imposed:

$$x = x_L: \quad \lambda\frac{\partial T}{\partial x} = 0, \quad G_s = A(T_s)G_0. \tag{3.14}$$

In the case of surface energy absorption the heat transfer equation does not contain the term $\partial G/\partial x$, and the equation for radiation transfer is not required. Laser source influence is introduced through the system (3.6), expressing energy conservation.

Taking into consideration the above statements, the mathematical model describing the behavior of solid phase (s) and liquid phase (l) and accounting for phase transitions can be written as follows:

$$\begin{gathered}\left[C_p(T)\rho\frac{\partial T}{\partial t}\right]_k = \left[\frac{\partial}{\partial x}\lambda(T)\frac{\partial T}{\partial x} - \frac{\partial G}{\partial x}\right]_k, \quad k = s, l \\ \left[\frac{\partial G}{\partial x} + \kappa G\right]_k = 0, \quad x_0 < x < x_L\end{gathered} \tag{3.15}$$

with boundary conditions:

$$t = 0: \quad T(x, 0) = T_0$$

$$x = x_0: \quad \lambda\frac{\partial T}{\partial x} = 0$$

$$x = \Gamma_{sl}: \quad \lambda_s\frac{\partial T_s}{\partial x} - \lambda_l\frac{\partial T_l}{\partial x} = \rho_s L_m v_{sl}, \quad T_s = T_l = T_m$$

$$x = \Gamma_{lv}: \quad \lambda_l\frac{\partial T_l}{\partial x} = \rho_l L_v v_{lv}, \quad G_s = A(T_s)\,G_0\exp\left(-\left(\frac{t}{\tau}\right)^2\right)$$

$$\rho_l v_{lv} = \rho_v(v_{lv} - u)$$

$$P_l + \rho_l v_{lv}^2 = P_v + \rho_v(v_{lv} - u)^2 \tag{3.16}$$

$$T_v = T_l \cdot \left\{ \left[1 + f^2 \left(\frac{\gamma - 1}{\gamma + 1} \right) \mathrm{M}^2 \right]^{1/2} - f \cdot \left(\frac{\gamma - 1}{\gamma + 1} \right) \mathrm{M} \right\}^2$$

$$\rho_v = \frac{1}{2} \rho_H \left\{ \left(\frac{T_l}{T_v} \right)^{1/2} \left[(\gamma \mathrm{M}^2 + 1) \exp(b^2 \mathrm{M}^2) \operatorname{erfc}(b\mathrm{M}) - \frac{4f}{\pi} \mathrm{M} \right] + \frac{T_l}{T_v} [1 - 2 \cdot f \cdot \mathrm{M} \exp(b^2 \mathrm{M}^2) \operatorname{erfc}(b\mathrm{M})] \right\}$$

$$P_H = R \rho_H T_l, \; P_H = p_b \exp\left(\frac{L_v}{R T_l} \left(1 - \frac{T_b}{T_l} \right) \right)$$

Let us formulate the method for numerical solution with dynamic adaptation as applied to system (3.15), (3.16). Transition to non-stationary system of coordinates is done by a substitution of variables of general type

$$x = f(q, \tau), \; t = \tau,$$

having the reverse transformation

$$q = \Phi(x, t), \; \tau = t.$$

Partial derivatives of dependent variables are expressed conventionally:

$$\frac{\partial}{\partial t} = \frac{\partial}{\partial \tau} + \frac{\partial q}{\partial \tau} \frac{\partial}{\partial q} = \frac{\partial}{\partial \tau} - \frac{\partial x}{\partial \tau} \frac{\rho}{\Psi} \frac{\partial}{\partial q} = \frac{\partial}{\partial \tau} + \frac{Q}{\Psi} \frac{\partial}{\partial q}$$

$$\frac{\partial}{\partial x} = \frac{\partial q}{\partial x} \frac{\partial}{\partial q} = \frac{\rho}{\Psi} \frac{\partial}{\partial q}, \quad \Psi = \frac{\partial x}{\partial q} \rho$$

where $\frac{\partial x}{\partial \tau} = -\frac{Q}{\rho}$ is the velocity of coordinates system movement, Q is a function depending on the solution to be determined, Ψ is a metric coefficient of transformation that shows how much the region is changed in comparison with initial region.

Using variables substitution, the mathematical model (3.15), (3.16) takes the form

$$\left[\frac{\partial (H\Psi)}{\partial \tau} \right]_k = \left[\frac{\partial W}{\partial q} - \frac{\partial (QH)}{\partial q} - \frac{\partial G}{\partial q} \right]_k, \; H = C_p T \tag{3.17}$$

$$\left[\frac{\partial G}{\partial q} + \kappa \rho \Psi G = 0 \right]_k, \; k = s, l, \; W = -\frac{\rho \lambda \partial T}{\Psi \partial q} \tag{3.18}$$

$$\left[\frac{\partial \Psi}{\partial \tau} = -\frac{\partial Q}{\partial q} \right]_k, \; \frac{\Psi}{\rho} = \frac{\partial x}{\partial q}, \; k = s, l, \; q_0 < q < q_L \tag{3.19}$$

with boundary conditions:

$$t = 0: \; T(q, 0) = T_0$$

$$q = q_0: \; \frac{\lambda \rho}{\Psi} \frac{\partial T}{\partial q} = 0, \; Q = 0 \tag{3.20}$$

$$q = \Gamma_{sl}: \quad T_s = T_l = T_m, \quad Q_{sl} = -\rho_s v_{sl}, \quad Q_{sl} = -\frac{W_s - W_l}{L_m} \tag{3.21}$$

$$q = \Gamma_{lv}: \quad \frac{\lambda_l \rho_l}{\Psi_l}\frac{\partial T_l}{\partial q} = -L_v Q_{lv},$$

$$G_s = A(T_s) G_0 \exp\left(-\left(\frac{t}{\tau}\right)^2\right),$$

$$\rho_l v_{lv} = \rho_v (v_{lv} - u), \quad Q_{lv} = -\rho_l v_{lv}, \tag{3.22}$$

$$P_l + \rho_l v_{lv}^2 = P_v + \rho_v (v_{lv} - u)^2,$$

$$T_v = T_l \cdot \left\{\left[1 + f^2\left(\frac{\gamma - 1}{\gamma + 1}\right)\mathrm{M}^2\right] - f \cdot \left(\frac{\gamma - 1}{\gamma + 1}\right)\mathrm{M}\right\}^2,$$

$$\rho_v = \frac{1}{2}\rho_H \left\{\left(\frac{T_l}{T_v}\right)^{1/2}\left[(\gamma \mathrm{M}^2 + 1)\exp(b^2\mathrm{M}^2)\operatorname{erfc}(b\mathrm{M}) - \frac{4f}{\pi}\mathrm{M}\right]\right.$$

$$\left. + \frac{T_l}{T_v}\left[1 - 2 \cdot f \cdot \mathrm{M}\exp(b^2\mathrm{M}^2)\operatorname{erfc}(b\mathrm{M})\right]\right\}$$

Equation (3.19) is the equation of reverse transformation. Function Q in this equation, as was already noticed, is to be chosen depending on the properties of the solution to be determined, thus permitting a great flexibility of the method. Without considering the selection of function Q in detail (a special analysis of this question is performed in [65]), we just observe that for any given form of Q, we obtain a different transformation. For example, choosing Q dependent on the spatial rate of change of the solution it is possible to increase the number of grid points in the region of large gradients [63–65]. For free boundaries problems the most important form is $Q = -D \cdot (\partial \Psi / \partial q)$ which provides a quasi-uniform grid at each time step if a sufficiently large value is chosen for the coefficient D. Thus, the problem for moving interface boundaries in computational space leads to the determination of values Q_{sl}, Q_{lv}.

To construct discrete models approximating the differential form of the problem (3.17)–(3.22), computational grids W_i^j must be introduced into each phase sub-region. In the solid phase computational grids are used with non-uniform step, h_i, along spatial variable q and step $\Delta\tau^j$ along variable τ:

$$\omega = \{(q_i, \Delta\tau^j), (q_{i+1/2}, \Delta\tau^j),$$

$$q_{i+1} = q_i + h_i, \quad q_{i+1/2} = q_i + 0.5h_i, \quad \tau^{j+1} = \tau^j + \Delta\tau^j,$$

$$i = 0, 1, \ldots, N, \; j = 0, 1, \ldots, J\}$$

In the region occupied by the liquid phase, a grid uniform in space is used.

Discretization in each sub-region is done by implicit conservative difference schemes [2]:

$$\left[\frac{(\Psi H)_{i+1/2}^{j+1}-(\Psi H)_{i+1/2}^{j}}{\Delta\tau^{j+1}}=\frac{W_{i+1}^{j+1}-W_{i}^{j+1}}{h_i}-\frac{(QH)_{i+1}^{j+1}-(QH)_{i}^{j+1}}{h_i}-\frac{G_{i+1}-G_i}{h_i}\right]_k,$$

$$\left[\frac{\Psi_{i+1/2}^{j+1}-\Psi_{i+1/2}^{j}}{\Delta\tau^{j+1}}=-\frac{Q_{i+1}^{j+1}-Q_{i}^{j+1}}{h_i}\right]_k,$$

$$\left[\frac{G_{i+1}-G_i}{h_i}+\kappa(\Psi\rho G)_{i+1}=0\right]_k^{j+1},\quad k=s,l, \tag{3.23}$$

$$\frac{x_{i+1}^{j+1}-x_i^{j+1}}{h_i}=\frac{\Psi_{i+1/2}^{j+1}}{\rho_{i+1/2}^{j+1}},\quad Q_i^j=-D\,\frac{\Psi_{i+1/2}^{j}-\Psi_{i-1/2}^{j}}{0.5(h_i+h_{i-1})},$$

$$W_i^j=-\left[\frac{\lambda_i^j\rho_i^j}{\Psi_i^j}\cdot\left(\frac{T_{i+1/2}^j-T_{i-1/2}^j}{0.5(h_i+h_{i-1})}\right)\right],\ i=0,1,\ldots,N-1$$

Functions W_i^j, Q_i^j, x_i^j, λ^j, $C_{\mathrm{p}i}^j$ are related to nodes, and $T_{i+1/2}^j$, $\Psi_{i+1/2}^j$ to points between nodes.

Values T_i^j, Ψ_i^j in nodes are determined through the value of these functions in points between nodes with the interpolation formula:

$$y_i^j=\frac{\rho_{i+1/2}^j\Psi_{i-1/2}^j h_{i-1/2}y_{i+1/2}^j+h_{i+1/2}y_{i-1/2}^j\Psi_{i+1/2}^j\rho_{i-1/2}^j}{\rho_{i+1/2}^j\Psi_{i-1/2}^j h_{i-1/2}+h_{i+1/2}\Psi_{i+1/2}^j\rho_{i-1/2}^j}.$$

Boundary conditions (3.20)–(3.22) are approximated by the following finite difference relations:

$$q=q_0:\ W_0^j=0,\ Q_0^j=0$$

$$q=\Gamma_{sl}:\ T_s^j=T_l^j=T_m,\ Q_{sl}^j=-\rho_s v_{sl}^j,\ Q_{sl}^j=-\frac{W_s^j-W_l^j}{L_m}$$

$$q=\Gamma_{lv}:\ W_i^j=-L_v Q_{lv}^j,\ Q_{lv}^j=-v_{lv}^j\rho_l^j,$$

$$\rho_l v_{lv}^j=\rho_v^j(v_{lv}^j-u^j),\ G_s^j=A(T_s^j)G_0\exp\left(-\left(\frac{t}{\tau}\right)^2\right),$$

$$P_l^j=P_v^j+\rho_v^j(v_{lv}^j-u^j)^2-\rho_l^j v_{lv}^{j2},$$

$$T_v^j=T_l^j\cdot\left\{\left[1+f^2\left(\frac{\gamma-1}{\gamma+1}\right)\mathrm{M}^2\right]^{1/2}-f\cdot\left(\frac{\gamma-1}{\gamma+1}\right)\mathrm{M}\right\}^2,$$

$$\rho_v^j=\frac{1}{2}\rho_H^j\left\{\left(\frac{T_l^j}{T_v^j}\right)^{1/2}\left[(\gamma\mathrm{M}^2+1)\exp(b^2\mathrm{M}^2)\,\mathrm{erfc}(b\mathrm{M})-\frac{4f}{\pi}\mathrm{M}\right]\right.$$
$$\left.+\frac{T_l^j}{T_v^j}\left[1-2\cdot f\cdot\mathrm{M}\exp(b^2\mathrm{M}^2)\,\mathrm{erfc}(b\mathrm{M})\right]\right\},$$

$$P_H^j=R\rho_H^j T_l^j,\ P_H^j=p_b\exp\left(\frac{L_v}{RT_l^j}\left(1-\frac{T_b}{T_l^j}\right)\right),$$

$$P_v^j=R\rho_v^j T_v^j$$

Algorithm of solution

The application of dynamic adaptation allowed to develop numerical algorithm the main idea of which is to make calculations according to homogeneous scheme (as in the smoothing methods) with simultaneous front tracking. For this purpose the solution of difference scheme (3.23) at one time step τ^j is done by means of two included iteration cycles. In the first boundary condition the values Q_{sl} and Q_{lv} are determined by means of iteration procedures which is equivalent to the determination of the values of interfaces velocity v_{sl}, v_{lv}. In the second cycle for both regions the values T_i^j and Ψ_i^j are determined by the usual method of three-diagonal matrices combined with Newton–Raphson method. Iterations are performed to fulfill the conditions:

$$|\delta\Psi_i^s| = |\Psi_i^{s+1} - \Psi_i^s| < \varepsilon_1 \Psi_i^s + \varepsilon_2$$

$$\varepsilon_1 \div \varepsilon_4 \leq 10^{-3}\text{–}10^{-6}$$

$$|\delta T_i^s| = |T_i^{s+1} - T_i^s| < \varepsilon_3 T_i^s + \varepsilon_4$$

Certain difficulties can arise when a new phase appears. In the above method a new region is introduced according to the following criteria. Overheating of the solid phase surface is admitted up to 0.2 K. It is assumed that the energy stored for overheating is utilized to form liquid phase. Comparing its value with L_m the initial liquid thickness and initial melting velocity v_{sl} are determined. Surface temperature is chosen so that the energy stored is sufficiently large for several atomic layers to melt. Usually, the initial thickness of the liquid phase is 8–100 Å.

The above procedure is used for mathematical modeling of laser melting and evaporation of condensed media [79, 81]. As an example, we consider the influence modes typical for metal cutting and for evaporation of ceramics [79].

In the first example, a laser pulse of rectangular shape with half-width 10^{-2} s and intensity $2 \cdot 10^5$ W/cm^2 is incident upon aluminum sample surface of thickness 1 cm. Energy absorption is assumed to be confined at the surface. The portion of absorbed radiation is characterized by some temperature dependence $A(T_s)$ together with $C_p(T)$ and $\lambda(T)$ which are shown in Fig. 6. When phase transition takes place all these values change abruptly, i.e., they experience a discontinuity. Note that one of the advantages of the proposed method is the possibility of working with discontinuous thermodynamical and optical characteristics without any smoothing.

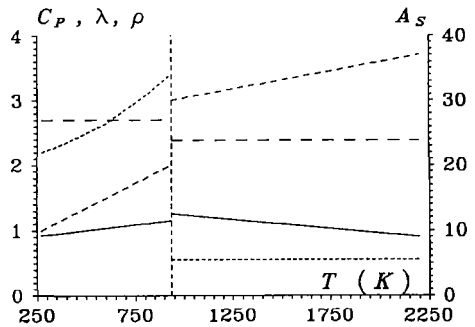

Fig. 6. ----- λ, W/(cm·K); — — — ρ, g/cm^3; ——— C_P, J/(g·K); ----- A, %

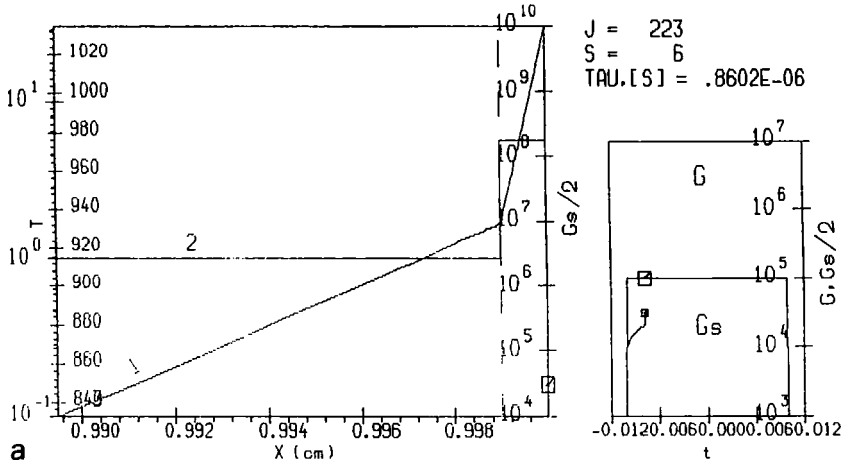
J = 223
S = 6
TAU,[S] = .8602E-06
T
Gs/2
G
Gs
G,Gs/2
X (cm)
t
a

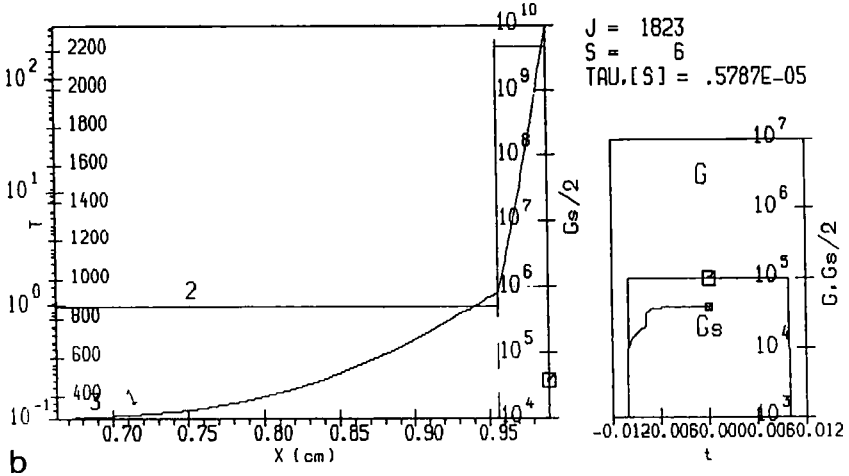
J = 1823
S = 6
TAU,[S] = .5787E-05
T
Gs/2
G
Gs
G,Gs/2
X (cm)
t
b

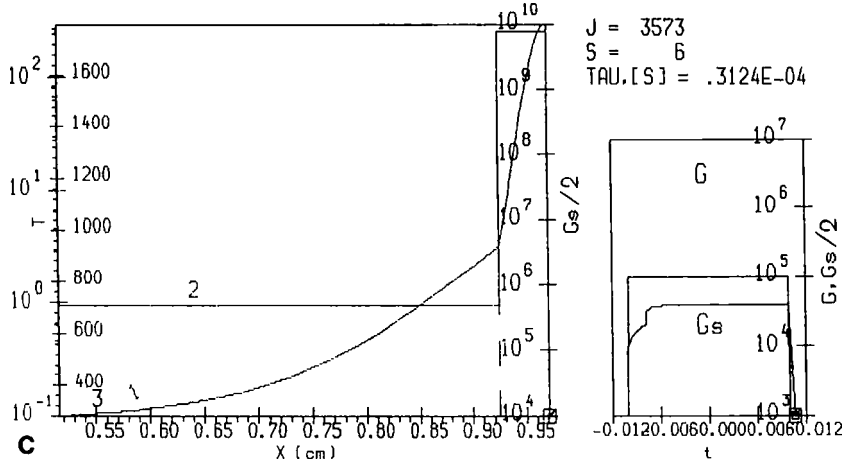
J = 3573
S = 6
TAU,[S] = .3124E-04
T
Gs/2
G
Gs
G,Gs/2
X (cm)
t
c

This feature allows to sharply increase calculations accuracy in the field of phase transformations.

In Fig. 7a–c the typical profiles of $T(x)$, $\Psi(x)$ are shown (and $G(x)$, in case of volumetric source), together with $G(t)$, $G_s(t)$ as displayed on monitor screen. The plot on the left characterizes the spatial distribution of temperature fields $T_s(x)$, $T_l(x)$ and functions $\Psi_s(x)$, $\Psi_l(x)$. Variation of functions $\Psi_s(x)$ and $\Psi_l(x)$ shows the dynamics of solid and liquid domains. On the right hand side, time-base of laser pulse $G(t)$ and portions of radiation absorbed by surface, $G_s(t)$, are given. Markers on these curves show the current time instant. In the upper right corner the values of current time, t, the number of time steps, J, and integration step, $\Delta\tau^j$, are given. In the legend, the current values of t^j, x_l, v_{sl}, x_v, v_{lv}, P_l are quoted.

The appearance of melting (Fig. 7a), accompanied by the introduction of new area is characterized by a sharp break in the diagram of $T(x)$ on the interface, which is marked by a vertical dashed line in the figures. The dynamics of solid and liquid phase size is defined by function $\Psi(x)$. In the solid phase $\Psi_s(x)$ decreases from 1 at the moment of melting to zero with complete melt. In liquid phase $\Psi_l(x)$ increases from 1 at the moment of melting to several orders (10^2–10^5) (Fig. 7b and c) depending on the sample thickness in the initial state and on the duration of the melting process. In Fig. 9 the temperature distribution at the moment of laser pulse end is shown. In Fig. 8a and b, the functions $G_s(t)$, $T_s(t)$, $v_{sl}(t)$, $v_{lv}(t)$ and $\Psi_l(t)$, characterizing the process dynamics are given. The negative branch of $v_{sl}(t)$ corresponds to melting, while the positive one is related to crystallization. The interfaces velocities are rather small (tens of centimeters per second) that is primarily due to the given intensity value, G. The maximum melt thickness reaches 0.5 cm and the evaporated layer is 0.03 cm.

In the second example we consider pulse influence of laser radiation on ceramics. At present, intensive studies in the field of the application of superconducting ceramics are carried out. Treatments such as laser annealing of ceramics are also widely used for the purpose of obtaining specific properties and for the formation of thin superconducting films produced by laser evaporation. Typically, it is very hard to predict the outcome of such processes, mainly because of the fact that the underlying physics is not known completely. Ceramics are materials with complex chemical composition and with badly studied optical and thermodynamical parameters and consequently it is difficult to determine the optimal modes of influence. The importance of mathematical modeling in the study of such phenomena is considerably increased.

As an example, let us consider the typical mode for pulse laser evaporation of ceramics, series $YBa_2Cu_3O_{7-x}$. From the experience it is known that optical and thermodynamical properties depend poorly on temperature and their values are within the range $\kappa = 10^4$–$10^5\,\mathrm{cm}^{-1}$, $C_p = (3\text{–}8)\cdot 10^{-1}$ J/(K g), $\lambda = (1\text{–}5)\cdot 10^{-2}$ W/(cm K). Thus, in comparison with metals, ceramics are materials

Fig. 7a–c. 1, T; 2, Ψ; 3, G. **a** Time $= -7.76\cdot 10^{-3}$ s, $x_l = 8.42\cdot 10^{-6}$ m, $x_v = 1.51\cdot 10^{-15}$ m, $v_{sl} = -0.175$ m/s, $v_{lv} = -7.63\cdot 10^{-11}$ m/s, $P_l = 9.46\cdot 10^{-11}$ bar. **b** Time $= 1.13\cdot 10^{-4}$ s, $x_l = 3.36\cdot 10^{-4}$ m, $x_v = 1.02\cdot 10^{-4}$ m, $v_{sl} = -3.32\cdot 10^{-2}$ m/s, $v_{lv} = -1.81\cdot 10^{-2}$ m/s, $P_l = 3.38\cdot 10^{-2}$ bar. **c** Time $= 1.07\cdot 10^{-2}$ s, $x_l = 4.49\cdot 10^{-4}$ m, $x_v = 2.95\cdot 10^{-4}$ m, $v_{sl} = -2.47\cdot 10^{-2}$ m/s, $v_{lv} = -5.78\cdot 10^{-4}$ m/s, $P_l = 9.98\cdot 10^{-4}$ bar

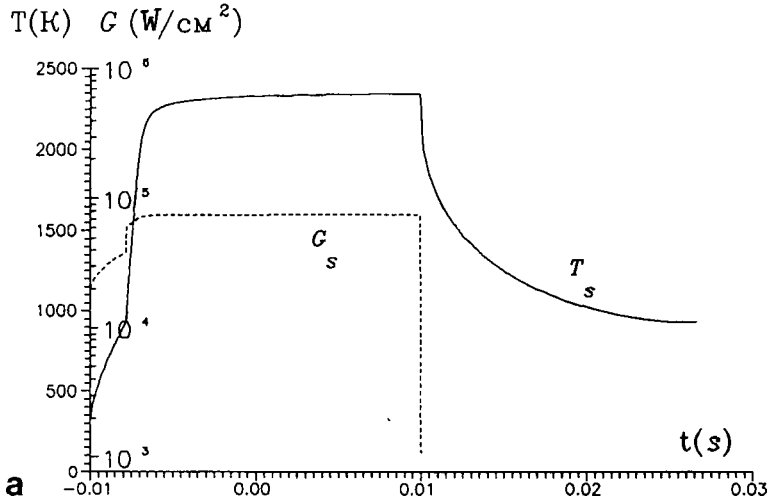
T(K) G (W/cm 2)
2500
2000
1500
1000
500
0
10 6
10 5
10 4
10 3
G s
T s
t(s)
-0.01
0.00
0.01
0.02
0.03
a

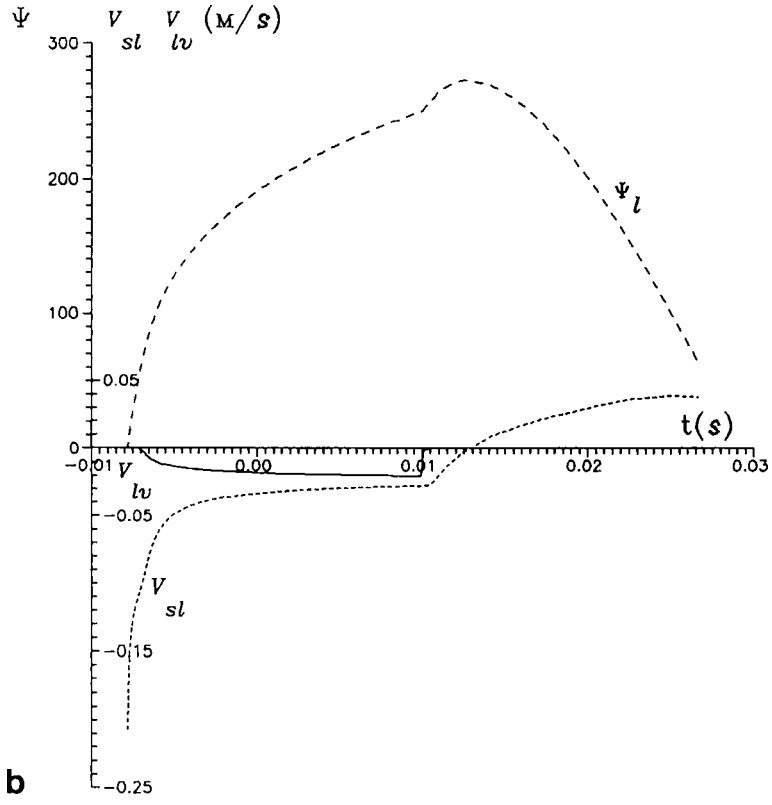
Ψ V sl V lv (M/s)
300
200
100
0
0.05
-0.05
-0.15
-0.25
Ψ l
t(s)
-0.01
0.00
0.01
0.02
0.03
V lv
V sl
b

Fig. 8

with low, thermal diffusivity, a, and relatively high absorption coefficients, κ. The experiments show that ceramics, series $YBa_2Cu_3O_{7-x}$, evaporates passing through melting state, i.e., as most metals do. However, the absorption of laser energy in ceramics is substantially volumetric, due to the different relation between the parameters a and κ.

In calculations, because of the absence of reliable data on optical and thermodynamical parameters, all the values were taken constant and the same for both phases. Their values were assumed to be equal:

$T_m = 1300$ K, $T_v = 2000$ K, $L_m = 2.5 \cdot 10^2$ J/g, $L_v = 6 \cdot 10^3$ J/g.

$\rho_s = \rho_l = 6.43$ g/cm^3, $\lambda_s = \lambda_l = 3 \cdot 10^{-2}$ W/(cm K), $A_s = A_l = 80\%$,

$C_{p_s} = C_{p_l} = 5 \cdot 10^{-1}$ J/g K, $\kappa = 5 \cdot 10^4$ cm^{-1}.

Let us consider some peculiarities of melting and evaporation of ceramics, thickness 5 μm, by laser pulse with $\tau = 50$ ns and $G_0 = 10^7$ W/cm^2. The temperature profile, $T(x)$, characteristic of volumetric source and fixed at time instant preceding appearance of the liquid phase, is shown in Fig. 9a. The given profile, $T(x)$, differs from the analogous one obtained during surface source influence by a smoother distribution in space and lower spatial gradients resulting in slower increase of melting velocity, V_{sl}. Melting process proceeds from the surface and rapidly leads to the formation of a temperature maximum which, in the solid phase and with volumetric source shown in Fig. 9b and c, reaches 50 K over the equilibrium temperature, T_m. As a result, a region, whose size is about 0.5 μm, is formed where the solid is in overheated metastable state. The size of overheated regions and the degree of overheating depend on thermal conductivity, absorptivity and on the source intensity. During heating, the liquid phase rapidly increases in size from 8 Å at the moment of melting to 0.1 μm in the middle of the pulse (Fig. 9c). The increase of liquid phase thickness leads to the fact that a great portion of radiation is absorbed in the liquid, resulting in its further heating, up to the evaporation temperature, T_v. At the same time, a smaller portion of radiation reaches the solid phase and the overheating degree is decreased under the influence of thermal conductivity till complete disappearance. In the liquid phase surface evaporation and volumetric energy absorption lead to the formation of a new metastable region with maximum temperature at a certain distance from the surface (Fig. 9c). Contrary to solid phase overheating, the metastable state in liquid is maintained till pulse end.

It is necessary to note that in the model (3.15)–(3.16) here used, the processes for volumetric nucleation and volumetric vapor formation are not considered. Moreover, it is supposed that the metastable phase is stable enough and has no time to decay during pulse influence. Therefore, the above calculations have the main purpose of attracting investigators attention to the possibility that metastable states appear in deep regions during laser treatment. More attentive study of such phenomena requires, first, additional experimental investigations and the development of more sophisticated mathematical models. The practical importance of the mathematical model discussed above consists mainly in the fact that it allows to determine the conditions for the formation of metastable states. And though their

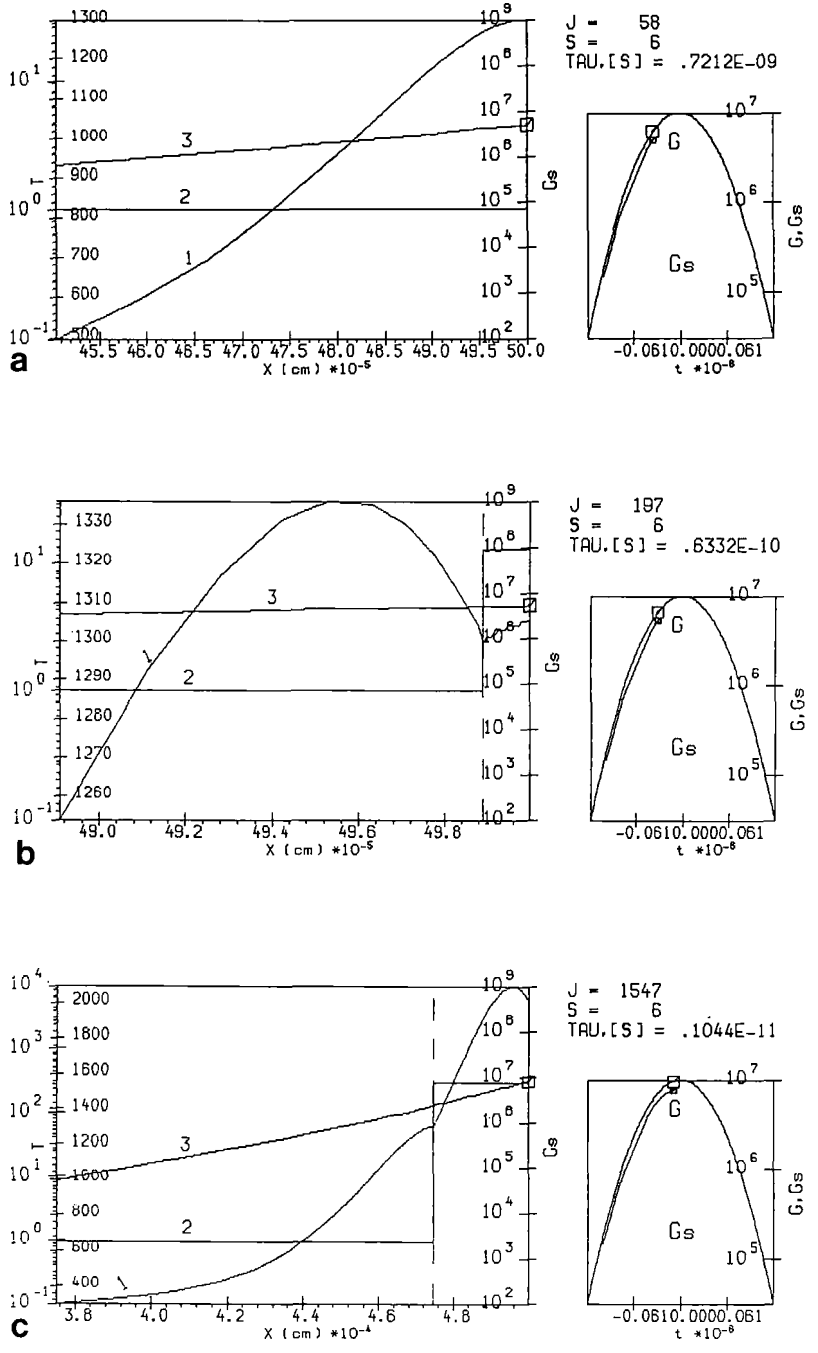

Fig. 9a–c. 1, T; 2, Ψ; 3, G. **a** Time $= -3.51 \cdot 10^{-8}$ s, $x_l = x_v = 0$ m, $v_{sl} = v_{lv} = 0$ m/s, $P_l = 0$ bar; **b** Time $= -3.24 \cdot 10^{-8}$ s, $x_l = 7.22 \cdot 10^{-9}$ m, $x_v = 3.66 \cdot 10^{-21}$ m, $v_{sl} = -0.61$ m/s, $v_{lv} = 1.4 \cdot 10^{-19}$ m/s, $P_l = 1.9 \cdot 10^{-19}$ bar; **c** Time $= -9.18 \cdot 10^{-9}$ s, $x_l = 2.52 \cdot 10^{-7}$ m, $x_v = 6.53 \cdot 10^{-13}$ m, $v_{sl} = -0.852$ m/s, $v_{lv} = -0.297$ m/s, $P_l = 0.52$ bar

lifetime is unknown, it is always finite. Therefore, explosive decay of metastable phase due to volumetric vapor formation processes is actually possible. It is necessary to consider its possible occurrence for a more correct development and application of laser technologies, since an explosive decay of metastable states is capable not only to accelerate the material elimination process, but also to present a serious problem during thin film coating and the production of elements of submicron sizes.

3.10 The problem of overheated metal melting [80]

As it was already noticed, metastable states nowadays attract the attention of many investigators. A great number of papers is devoted to formation dynamics and the properties of overcooled and frozen states of condensed substance [82–84]. The properties of solid bodies overheating during pulse influence are more complicated and less studied. The main efforts in the theoretical study of this subject should be directed, first, to the construction of more comprehensive mathematical models, since, for example, the classic version of the Stefan problem in the given situation is far from being a correct description of the problem. Actually, during strong overheating, the velocity in the problem (3.1–3.3) can be formally taken infinite. As a consequence one obtains the self-similar solution of the one-space-dimensional melting problem in which the initial temperature, $T_0 > T_m$, exceeds melting temperature. In this case for the temperature profile and the velocity of front movement the following expressions are obtained [8]:

$$T_s = T_0 - C\Phi(x/X_m), \quad T_l = T_m$$

$$X_m = 2\beta(at)^{1/2}, \quad a = \lambda/(C_p\rho),$$

$$v_{sl} = \mathrm{d}X_m/\mathrm{d}t = \beta(a/t)^{1/2}, \quad \Phi = 2/\pi^{1/2}\int_z^\infty \exp(-y^2)\,\mathrm{d}y,$$

where β is a parameter.

During high overheating, when $T_0 - T_m = L_m/C_p$, this solution becomes completely meaningless. Correct mathematical description of such physical situation requires the use of the complete system of hydrodynamic equations [80] as unlimited increase of velocity, v_{sl}, at the initial time moment would result in unlimited value of pressure P in the system. For a number of materials, the dependence of phase transformation temperature on pressure, $T_m(P)$, is experimentally established [85]. A precise consideration of this phenomena should lead to establish bounds for the initial velocity, v_{sl}, and to the elimination of nonphysical regions.

A mathematical model considering hydrodynamical effects and including the relationship, $T_m = T_m(P)$, has the form (3.8).

The boundary conditions can be specified as follows. The left end of bar, $X = X_0$, is rigidly fixed and heat impermeable, i.e., the conditions correspond to:

$$u = 0, \quad \frac{\partial T}{\partial x} = 0. \tag{3.24}$$

The right end of bar, $X = X_N$, is assumed to be free and also thermally insulated;

$$p = 0, \quad \frac{\partial T}{\partial x} = 0. \tag{3.25}$$

On the interface, $X = \Gamma_{sl}$, three conservation laws are fulfilled and the law for melting temperature change is given, depending on pressure:

$$\begin{gathered} \rho_s \cdot v_{sl} = \rho_l \cdot (U_s - U_l + v_{sl}), \\ \rho_s \cdot v_{sl}^2 + P_s = \rho_l \cdot (U_s - U_l + v_{sl})^2 + P_l, \\ \lambda_s \cdot \frac{\partial T_s}{\partial x} - \lambda_l \cdot \frac{\partial T_l}{\partial x} = L_m \cdot \rho_s \cdot v_{sl}, \\ T_{sl} = T_m(P_s). \end{gathered} \tag{3.26}$$

The initial conditions were chosen on the basis of the following considerations. It was supposed that a thin layer of the material is heated up to a temperature T_0, exceeding the equilibrium temperature, T_m, and the process of melting begins after the propagation of an unloading wave (the pressure in medium decreasing to zero). This situation is simulated by the equations of state in the form of $p_k = p_k(\rho - \rho_0, T - T_0)$ and spatial temperature distributions, $T(0, x)$, and density, $\rho(0, x)$, in the form of uniform step functions subject to jump at the interface:

$$\left.\begin{aligned} T(0, x) &= T_0 \\ \rho(0, x) &= \rho_s \\ u(0, x) &= 0 \end{aligned}\right\}, \; x_0 < x < \Gamma_{sl}, \quad \left.\begin{aligned} T(0, x) &= T_{sl} \\ \rho(0, x) &= \rho_l \\ u(0, x) &= u_l \end{aligned}\right\}, \; \Gamma_{sl} < x < x_N. \tag{3.27}$$

As thermodynamical parameters and state equations, in calculations the values typical for aluminum were used [86]:

$$\varepsilon_k = (C_p \cdot T)_k;$$

$$p_s = \tfrac{3}{2} \cdot P_{s0} \cdot (z_s^{7/3} - z_s^{5/3}) \cdot [1 + \alpha \cdot (z_s^{2/3} - 1)] + 3 \cdot R \cdot \rho \cdot (T_0 - T) \cdot [\gamma + 4 \cdot (z_s - 1)];$$

$$p_l = P_{l0} \cdot [z_l - 1 + \beta \cdot (T - T_{sl})], \; z_k = \rho/\rho_k, \; k = s, l,$$

where $T_m = 933.6$ K, $\rho_{s0} = 2.7$ g/cm^3, $\rho_{l0} = 2.383$ g/cm^3, $R = 0.30793$ J/(g·K),

$$P_{s0} = 7.27 \cdot 10^5 \text{ bar}, \; P_{l0} = 10^5 \text{ bar}, \; \alpha = 0.225, \; \gamma = 2.136, \; \beta = 3 \cdot 10^{-5} \text{ K}^{-1}.$$

For relationship, $T_{sl} = T_m(P_s)$, the experimental data [85] which were approximated by the expression were used:

$$T_{sl} = T_m + 0.00644 \cdot P_s.$$

Calculations begin with the solution of nonlinear system (3.26–3.27) from which the values T_{sl} and all related values were determined.

Simulation [80, 87] shows that consideration of hydrodynamic effects led to the limitation of phase boundary movement (Fig. 10a), thereby, within the range of overheating, $T = 50$–300 K, whose maximum value was less than sound velocity. The limitations of velocity, v_{sl}, are due to the appearance of high pressure on solid phase surface, shifting the temperature value $T_{sl} = T_m(P_s)$, to higher values, which in turn lowers temperature gradients on this surface and decreases the velocity v_{sl}. The decrease of v_{sl}, in turn, leads to the decrease of P_s and $T_m(P_s)$ (Fig. 10b) and at the moment in which the equality, $T_{sl} = T_m$ is attained, the interface pressure becomes zero and the velocity v_{sl} tends to that of a self-similar solution (Fig. 10a, dashed line). The pressure rise on interface is further spread into solid and liquid phases causing hydrodynamical disturbances which eventually determine the non-monotonous character of the behavior of $v_{sl}(t)$. In Fig. 10c and d, the change of pressures, P_s, P_l, and velocities U_s, U_l, are shown on the interface Γ_{sl}. Spatial distributions of temperature in both phases for various time instants are shown in

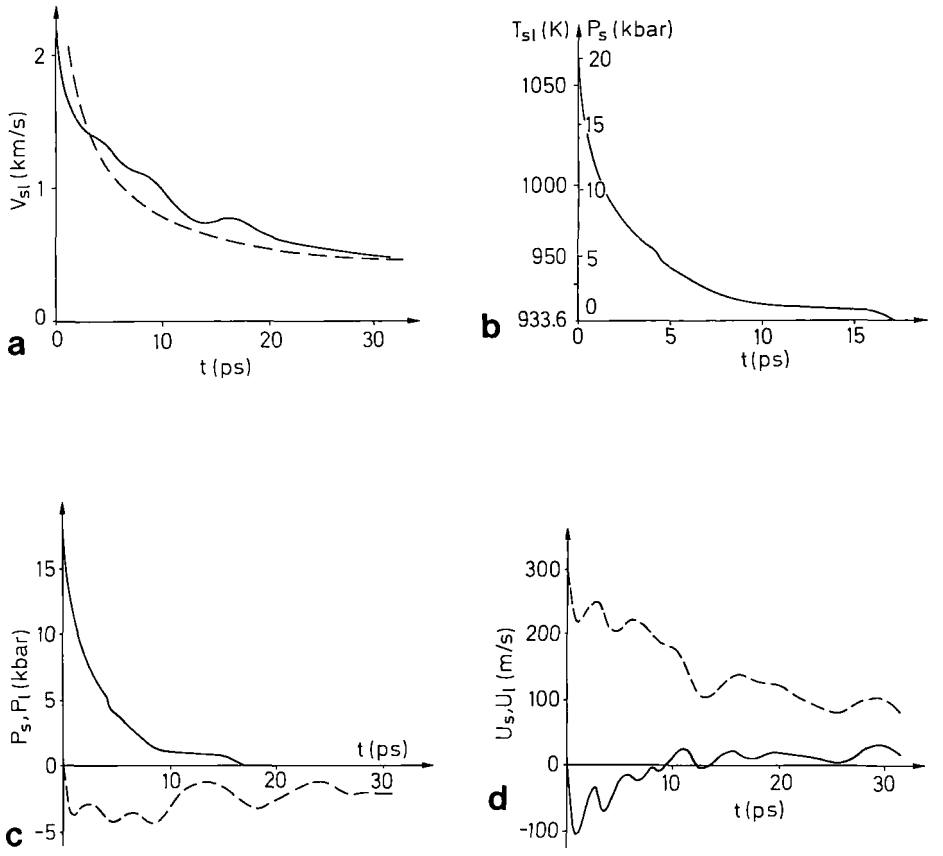

Fig. 10

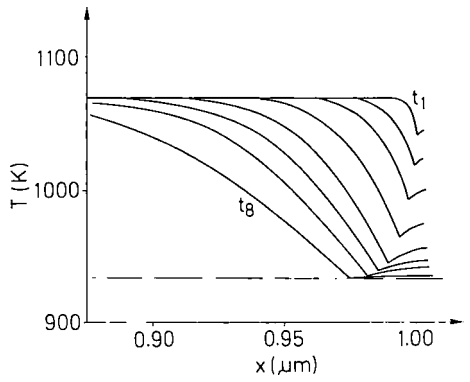

Fig. 11

Fig. 11. On temperature curves, a minimum corresponds to the interface position. Pressure and velocity on this boundary have jump discontinuities (Fig. 10c, d).

Note, that the application of a kinetic condition of the type (3.5) instead of (3.3) in an analogous statement leads to a solution completely different from a self-similar one.

In conclusion, we note that numerical solution of the problem (3.23)–(3.27) was carried out by the specially developed algorithm [87], based on the dynamic adaptation method and allowing explicit determination of interface position, like for the solution of the classic version of Stefan problem, and the calculations are carried out according to a homogeneous algorithm.

The principle of dynamically adapting grids is extended to the class of non-stationary problems of gas-dynamics [88, 89], allowing to determine explicitly weak and strong singularities, in particular, shock waves can be calculated without artificial viscosity. With no particular difficulty, the method is generalized to multi-dimensional problems of mathematical physics (see [62, 90, 91], where non-stationary two-space-dimensional problems and boundary layer problems have been considered.)

Thus, the development of the dynamic adaptation methods is a powerful tool for theoretical study of laser technology problems.

4 Laser surface modification and treatment of coatings

As has been noted, laser radiation with intensities higher than necessary for heat-treatment leads to the melting of thin surface layers. The melt being formed then can be cooled with a high rate due to heat removal to the bulk or artificially from the outside. Experiments [92, 93] show, that if the cooling rate exceeds the value of 10^6 K/s, then the crystallization front may be too slow to reach the surface, and a certain part of the melt appears to be frozen in an amorphous state. This phenomenon is the basis of the production process of surface amorphous layers in metal alloys and semiconductors [84, 94]. Such phenomenon has not been experimentally observed for pure metals.

If the operation of laser melting and subsequent crystallization is performed with the material previously coated with an appropriate substance, then laser melting leads to the formation of surface layers with a new composition, and, consequently, with different properties. This phenomenon underlies the technological process called laser surface modification or laser doping. Note, that for the surface modification (laser doping) the impurity need not necessarily be coated as a solid film, but can be supplied in the form of liquid or gas jet [1].

Similar processes are typical, also, for laser treatment of coating, in particular, for laser cladding. The coating of construction materials by solid layers is one of the procedures for improving wear resistance, durability and reliability of manufactures. However, the physical-chemical properties of metal films, coated onto the substrate surface by one of known methods, such as plasma or laser spraying, not always meet the necessary requirements. Depending on the materials used, the coating method and the thickness, the coatings can have weak adhesion, high porosity, laminated structure and other defects. Further laser treatment, leading to melting of the surface layers allows to remove most of the indicated defects. Then, the coated layer is melted in such a way to achieve the minimum melting of the basic material, as a considerable mixing can worsen the cladding layer properties. As cladding materials usually Co, Ni, Ti and iron based alloys are used. The method of solid layer coating is well enough tested and commonly used [1, 94].

One of the main problems to be solved by mathematic modeling in this area is the determination by numerical calculation of optimum values for laser radiation intensity and duration for the treatment of heterogeneous materials.

For the mathematical description of a multilayer material behavior under the pulse influence we write the heat transfer equation for each layer, complemented by appropriate boundary conditions on phase boundaries Γ_{sl} and on interfaces of the materials $\Gamma^{i,i+1}$, where indices i, s, l refer to i-th material, solid and liquid phases, respectively.

$$\left[\frac{\partial}{\partial t}(\rho C_p(T)T) = \frac{\partial}{\partial x}\lambda(T)\frac{\partial T}{\partial x}\right]_k^i \tag{4.1}$$

$$i = 1, 2, \ldots, N, \quad k = s, l$$

On the interfaces $\Gamma^{i,i+1}$ for (4.1) the so called contingency conditions or boundary conditions of the 4th type are written. For an ideal contact they reduce to the diffraction conditions:

$$\left[-\lambda(T)\frac{\partial T}{\partial x}\right]^i = \left[-\lambda(T)\frac{\partial T}{\partial x}\right]^{i+1}, \quad T^i = T^{i+1} \tag{4.2}$$

During heating of i-th material up to the melting point T_m^i the additional conditions on the phase boundary Γ_{sl}^i are:

$$\left[-\lambda(T)\frac{\partial T}{\partial x}\right]_s^i - \left[-\lambda(T)\frac{\partial T}{\partial x}\right]_l^i = \rho_s^i L_m^i v_{sl}^i$$
$$T_s^i = T_l^i = T_m^i \tag{4.3}$$

As a typical example of the coating laser treatment let us consider the problem of melting and vaporization of the two-layer material, comprising an aluminum substrate of thickness $l_{Al} = 1$ mm, on which a thin titanium film $l_{Ti} = 0.1$ μm is coated. The impinging pulse has a rectangular form, a duration $\tau = 5 \cdot 10^{-8}$ s and intensity $G = 5 \cdot 10^7$ W/cm^2. Thermodynamical characteristics and parameters of the two materials significantly differ from each other, and their reflectivity is not considered. Let us point out the main features of the conditions being considered.

Laser radiation is completely absorbed in the bulk of titanium. Aluminum, being under titanium, is heated by heat conduction. With the chosen influence parameters the first to be melted is aluminum, whose equilibrium melting point $T_m = 933$ K is almost three times lower than titanium melting point. In Fig. 12a and b the time dependence of melting–crystallization rates for aluminum $v_{sl}^{Al}(t)$ and titanium $v_{sl}^{Ti}(t)$ vaporization rates $v_{lv}(t)$ and the surface temperature $T_s(t)$ are presented. The negative branches of $v_{sl}^{Al}(t)$, $v_{sl}^{Ti}(t)$ curves correspond to melting, the positive ones to crystallization. The vertical dotted line describes the end of laser pulse. When the surface temperature $T_m^{Ti} = 2000$ K is reached the second melting front, characterized by the rate $v_{sl}^{Ti}(t)$, penetrates deeply into the titanium from the surface (Fig. 12b). The termination of laser pulse is followed by a sharp decrease of the surface temperature and vaporization stops (Fig. 12a). The quick heat transfer from titanium to aluminum leads to a further substrate melting and to the beginning of titanium crystallization. The crystallization proceeds with high rate, its maximum value is several times higher than the melting rate. The high rate of crystallization leads to a significant release of the crystallization energy in the liquid phase, which inhibits its cooling. This stage of the process is characterized by a plateau on the curve of the surface temperature $T_s(t)$ (Fig. 12a). On completion of the crystallization in titanium the surface cooling rate again increases, which eventually allows crystallization to start in aluminum. The maximum rate of aluminum crystallization, also, exceeds the maximum melting rate, as a consequence of the low heat conductivity of titanium in comparison with aluminum.

For comparison let us consider the same influence conditions, changing only one parameter, namely, increasing the coating thickness by a factor 2: $l_{Ti} = 0.2$ μm. In this case the development of the process qualitatively changes (Fig. 12c, d). Because of its low heat conductivity, as compared to aluminum, titanium is heated more rapidly than in the previous case and is the first to be melted. Aluminum melting begins with a considerable delay. By the pulse termination the surface vaporization rate v_{lv} is several times higher than in the previous case, the surface temperature and the melting rate v_{sl}^{Ti} are also significantly higher. The maximum crystallization rates v_{sl}^{Ti} and v_{sl}^{Al} are lower, although the surface temperature behavior (Fig. 12d) is qualitatively the same as in the first case. The significant quantitative differences of curves $v_{sl}^{Ti}(t)$ and $v_{sl}^{Al}(t)$ lead to considerable deviations in the depths of fusion of both materials.

The example considered shows that due to multiple interrelation of the influence parameters in problems of coating treatment even the qualitative stages of the process cannot be predicted without the use of appropriate mathematical models.

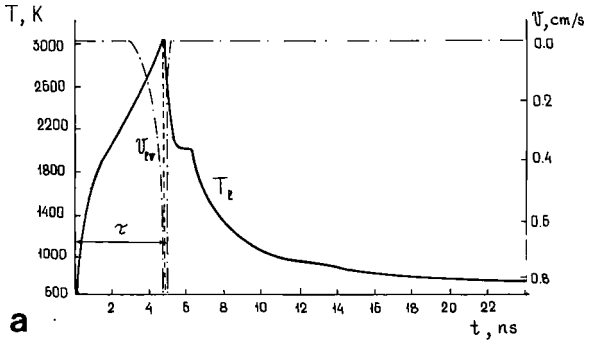
T, K
3000
2600
2200
1800
1400
1000
600
2 4 6 8 10 12 14 16 18 20 22
t, ns
V_{ev}
T_ℓ
τ
V, cm/s
0.0
0.2
0.4
0.6
0.8

a

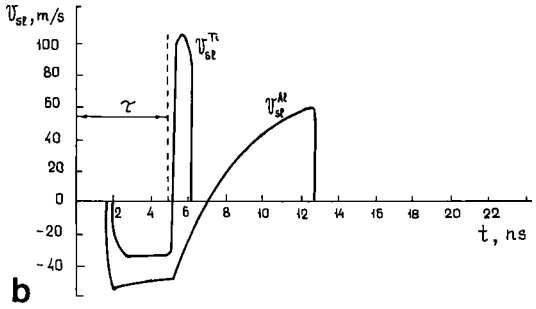
V_{sl}, m/s
100
80
60
40
20
0
-20
-40
2 4 6 8 10 12 14 16 18 20 22
t, ns
τ
V_{sl}^{Ti}
V_{sl}^{Al}

b

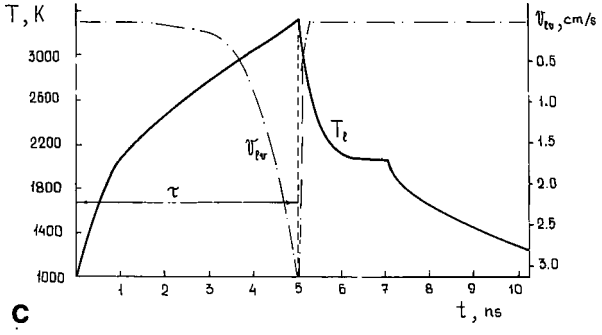
T, K
3000
2600
2200
1800
1400
1000
1 2 3 4 5 6 7 8 9 10
t, ns
V_{ev}
T_ℓ
τ
V_{ev}, cm/s
0.5
1.0
1.5
2.0
2.5
3.0

c

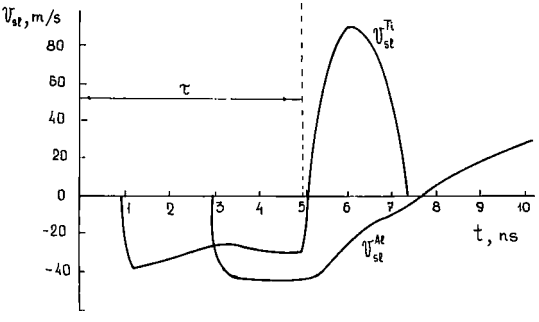
V_{sl}, m/s
80
60
40
20
0
-20
-40
1 2 3 4 5 6 7 8 9 10
t, ns
τ
V_{sl}^{Ti}
V_{sl}^{Al}

d

Fig. 12

Doping processes, in which one of the materials acts as an impurity, or similar processes under laser influence on the alloys, require more complex physical-mathematical models. The mathematical model for crystallization of multi-component systems, disregarding the hydrodynamics of the melt, usually is based on the heat transfer equation with the addition of equations describing the change of the components concentration during the crystallization process.

The formulation of the problem of laser pulse influence has a number of peculiarities. The main physical feature to be considered is the non-equilibrium of the process both at the melting and at the crystallization stage. It is known that the melting and crystallization are non-symmetric processes [61], under metastability conditions. The description of metastable states arising in melt was discussed in the previous section. Let us briefly consider the main aspects of physical-mathematical description of a multi-component melt undergoing non-equilibrium crystallization.

Non-equilibrium alloy crystallization is related, in the first place, to extremely high cooling rates and, respectively, high rates of phase front propagation. It is known [96, 97] that, depending on the cooling conditions, the same alloy can have a different morphological structure: regular, cellular or dendritic. Until recently in the description of the liquid alloy crystallization an assumption about the local thermodynamic equilibrium on the interface melt-crystal has been used, which is valid for crystallization rates not exceeding 1 m/s. In these cases the main problem is the determination of the temperature on the phase boundary, the composition being determined by solids and liquids lines of the phase diagram. The commonly well-known mathematical model in crystal equilibrium growth theory is, apparently, the concentration overcooling model of Mullins and Sekerka [98]. The basis of the model is the assumption that the movement of the crystallization front is so slow, that segregated impurity is mixed with liquid phase thanks to diffusion. The increase of the overcooling degree is due to decrease of the equilibrium temperature T_m of phase transition, caused by accumulation of the impurity in the melt near the crystallization surface. Under certain conditions the initial plane front becomes unstable and acquires a cellular or dendritic structure. The main achievement of the concentrational overcooling model is considered to be the possibility of reproducing critical condition for the transformation of a plane front into a cellular one. Other aspects of equilibrium crystallization are considered in [96, 97, 99, 100].

The experiments of last years [101–103] on crystallization of alloy melt thin layers after laser influence have shown that crystallization following exposure of the order of picoseconds can be performed with enormous rates 50–100 m/s, at which an assumption about local equilibrium is hardly valid. The studies [104–106] have shown the existence of a real deviation from equilibrium on the interface melt-crystal, where the impurity concentration significantly exceeds the equilibrium limit of solid body solubility, as the so called impurity capture occurs. A theoretical study on the high crystallization rate under such conditions requires a comprehensive examination of the kinetics and the phase front structure. The analysis of non-equilibrium processes of the high rate crystallization and their mathematical description have been carried out in a number of papers [107–109].

In spite of the high complexity of theoretical studies, laser doping and surface modification find common practical use in various technological cycles. As an

example, we shall dwell on laser hardening method of aluminum alloys, developed by the authors [110–112] and used for manufacturing of automobile motor pistons.

The technological process consists in metal powder coating on the piston surface and its subsequent fusion by laser radiation. The powders coating is performed by coverings. Fusion is achieved by laser radiation with wavelength $\lambda = 10.6\,\mu m$, $G = 10^4\,W/cm^2$ intensity and speed $v = 1\,m/s$. As a result of remelting in the radiation region a wear resistant aluminum alloy, differing from the basic metal both by structure and properties, was obtained. Then in the remelted zone the groove was turned for compression rings. In the process of the studies powders based on NiCr, FeCuB and NiCrMo were utilized. The tests have shown that the most efficient doping of Al_{25} alloy is achieved with powders based on NiCr. As a result of the doping an alloy with 2–3 times increased hardness, high temperature resistance and impact viscosity has been produced. The alloy produced at a high cooling rate has a fine dispersion structure with an oversaturated solid solution, which makes resistance characteristics several times higher. The method above has been introduced at a number of plants of automobile branch.

5 Laser cutting and dimensional treatment

Laser cutting of metal sheets with ≈ 1 cm thickness has significant advantages over other methods employing, e.g., oxygen–acetylene flames or plasma. The main ones are the high quality of cutting, the possibility of complex contour cutting, the high localization of heat influence. The best results are achieved on super-resistant and refractory materials for the purpose of drilling holes of given form, depth and diameter with high precision.

Laser cutting and dimensional treatment of metals are performed by melting and vaporization processes. The cutting of non-metals has considerable differences due to their high transparency and low heat conduction. For comparison note that heat conductivity λ of metals lies in a range of 0.1–5 W/(cm K) while for dielectrics it lies in 10^{-3}–10^{-2} W/(cm K). The coefficient of volumetric absorption for most metals is $\chi = 10^5$–$10^6\,cm^{-1}$, while for non-metals it is $\chi = 10^1$–$10^4\,cm^{-1}$. Therefore, the cutting of non metals is achieved, as a rule, either by sublimation, or as a result of generation in the bulk of the material of high thermal pressure, the so-called thermal cleavage.

With exclusion of thermal cleavage processes, for laser cutting, miniature welding and dimensional treatment the same mathematical models can be used including as a necessary element the phase transition dynamics of the first type.

5.1 Surface evaporation without plasma formation

In the present subsection we shall consider the principal steps of construction of the mathematical models for the specified processes and simulation results, obtained with their help. In describing pulse influence conditions the microscopic movement of the melt may be disregarded, and then the condensed medium behavior can be described by the heat transfer equation. The processes in the evaporated substance

are usually described by the system of gas-dynamics equations. The equations for the condensed and gaseous media are coupled through the boundary conditions on the phase boundary Γ_{lv}. The formulation of boundary conditions in the general case represents a complicated problem, as it is connected with the physics of intensive surface evaporation.

The vaporization process plays an extremely important role due to the relevant increase of energy capacity and of specific volume of the substance in the phase transition. Note, that vaporization can proceed in two considerably different conditions. If in the subcritical range of temperatures $T < T_c$ the ambient pressure p exceeds the pressure of saturated vapors $p > p_n$, then the phase transition occurs without the formation of an interface and can be described as a process in a continuum. A so-called gas-dynamic model of vaporization corresponds to these conditions [113]. The inequality $p > p_n$ represents a necessary condition for the applicability of vaporization gas-dynamic model. When $p < p_n$ in the vaporization region, a sharp phase boundary must exist, on which, besides the laws of mass, momentum and energy conservation, additional relationships determining the phase transition kinetics have to be formulated. A theoretical description of such vaporization conditions is performed in the framework of the one phase version of the Stefan problem, in which the temperature of the plane transition front has a weak logarithmic dependence on the front velocity [58]. The successive formulation of boundary conditions on the phase interface when vaporization has developed, requires, strictly speaking, the consideration of the kinetic equation. Intensive vaporization is followed by the appearance of a non-equilibrium Knudsen-layer, adjacent to the phase boundary. The hydrodynamics approach in this region is absolutely unacceptable, as the current parameters vary over a distance of the order of the mean free path. The Knudsen layer usually is considered as the gas-dynamic gap, the parameters of which from the external side are determined with some assumptions about the type of non-equilibrium distribution function inside the Knudsen layer. Depending on the assumption used, various mathematical models of Knudsen layer have been realized, from which the additional relationships at the vaporization front Γ_{lv} are determined [56, 59, 114–119].

The mathematical description of the surface vaporization process is considerably dependent on the conditions being considered. Usually it is assumed, that the vaporization rate has an upper bound $u \leq u_c$ or $\mathrm{M} = u/u_c \leq 1$, where $u_c = (\gamma RT)^{1/2}$ is the velocity of sound, and M is the Mach number. When the substance vaporizes under the influence of a continuous radiation current to the vacuum or to a medium with negligibly low pressure compared to saturation pressure, M is 1. In this case the behavior of condensed medium ceases to depend on the external gas-dynamics problem, which simplifies the description of vaporization process (3.15) considerably.

A more complex mathematical model is used for description of vaporization conditions with $\mathrm{M} < 1$. In this case the processes in condensed medium and in gas are correlated, the value of M is a priori unknown and must be considered as a quantity to be determined [120]. In this case the problem (3.15) must be considered together with the system of gas-dynamics equations, which in the

coordinate system moving with the phase interface Γ_{sl} is:

$$\begin{gathered}\frac{\partial \rho}{\partial t}+\frac{\partial}{\partial x}(\rho(u-v_{sl}))=0 \\ \frac{\partial(\rho u)}{\partial t}+\frac{\partial}{\partial x}(\rho u(u-v_{sl}))=\frac{\partial p}{\partial x} \\ \frac{\partial[\rho(\varepsilon+u^2/2)]}{\partial t}+\frac{\partial}{\partial x}[\rho(\varepsilon+u^2/2)(u-v_{sl})]=-\frac{\partial(pu)}{\partial x}\end{gathered} \tag{5.1}$$

So far the mathematical structure and the properties of the solutions of the nonlinear system describing such non-equilibrium processes, have not been studied in detail. At the same time, the problem of the condensed media vaporization under different non-stationary heating conditions are of great practical interest. The formulation of such problems is connected with a non-trivial question about the phase transition deviation from equilibrium, i.e., the behavior of M.

In vaporization into vacuum the change of M on the boundary of phase interface can be related to the heating of evaporated substance (plasma formation) or to quick variation of surface temperature caused, for instance, by a change of the source intensity G. Vaporization under these conditions has non-stationary nature, the main feature of which is the nonlinear dependence of phase transition kinetics on a number of parameters of the incident pulse, such as intensity, duration, change rate, etc. As the calculations [121, 122] have shown, the behavior of M, describing the deviation from equilibrium of the vaporization process, cannot be obtained by means of simple analytic evaluations, but the performance of numerical experiment is required. The mathematical modeling of aluminum surface vaporization in vacuum under various non-stationary heating conditions has shown that the vaporization process kinetics in this case appear to be more complex than it has been assumed earlier.

Let us consider the example of M depending on the heating conditions. In [123], the results of the numerical solution of the vaporization problem are presented for a two-phase system in the case of the heating of a condensed medium by a rectangular pulse of radiation with a microsecond duration. Based on these results the conclusion that M decreases without any restriction with the heating intensity reduction has been formulated. However, such a conclusion seems to be less justified, due to the reason that the results obtained for the concerned conditions cannot be reproduced for other cases of the intensity change. The numerical simulation of the process, made in papers [121, 122] with the help of the mathematical models (3.15), (5.1) under different influence conditions, has shown that the behavior of the parameter M in a more general case is qualitatively different from that described in [123]. In the analysis of the surface vaporization processes the same formulation and the same condensed medium characteristics (of aluminum) were used as in [123]. The value of M under boundary conditions was not fixed and was determined from the simultaneous solution of the heat transfer equation and gas-dynamics equations.

In Fig. 13, the graphs of M and p_H vs. time are presented. It can be noticed, that after switching off the source $G = 10^7$ W/cm^2 at the moment of time $t = 1\,\mu$s a rapid drop of M and p_H occurs. In this, M does not reach zero but passing through a minimum it begins to increase again unlike in [123], where M drops to zero and remains fixed on this level.

In Fig. 14a–c, the examples of immediate switching off the radiation source in various times are given. The intensity of the source G was assumed to be 10^7 W/cm^2. The intensity on the condensed medium surface was determined with the account of aluminum absorptivity $G = A(T_s) \cdot G$, where $A(T_s)$ was assumed to be

$$A(T_s) = \begin{cases} 0.23 & T_s \le T_m \\ 0.64 T_s^{0.4} & T_s > T_m. \end{cases}$$

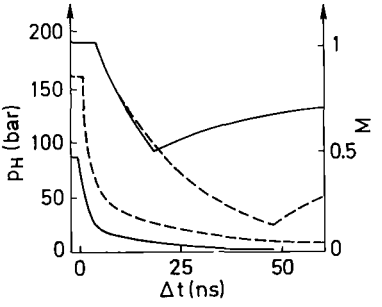

Fig. 13

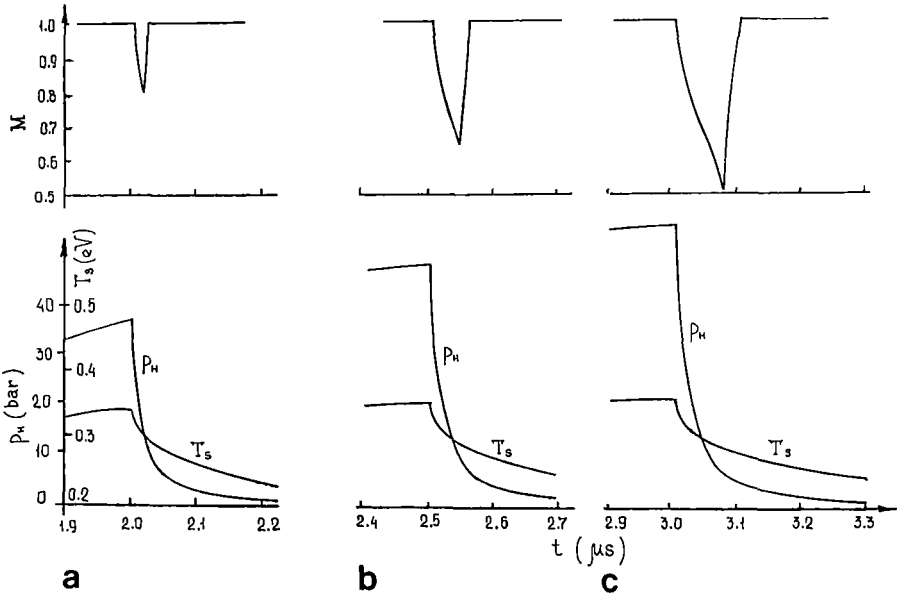

Fig. 14

The graphs in Fig. 14 show that with the increase of vaporization time the previously evaporated substance reaction intensifies, leading to faster drop of M.

In Fig. 15, the profiles of T_s, p_H, M are presented corresponding to a discontinuous change of G for various amplitudes. With a change of amplitude less than 20% the value of M does not change and is 1. It is notable, that in all cases in Figs. 14 and 15 M reaches the initial level M = 1.

Figure 16 shows the graph of M corresponding to the intensity modulation $G_s = G/(1 - a \cdot \sin(2\pi\Delta t/\tau))$, which was switched on after 2 μs from the pulse activation with intensity $G = 5 \cdot 10^8$ W/cm^2. The modulation period is $\tau = 20$ ns. The calculations have shown that M essentially does not depend on the modulation depth and, moreover, M becomes less than one after the significant intensity drop and stays there almost through the entire range of growth of G.

In the case $a = 0.5$ the change of M correlates with the order-of-magnitude of the linear evaluation [122]. However, with the decrease of modulation depth ΔM sharply decreases. With $a = 0.2$ the difference of M from 1 does not exceed 10^{-4}. This agrees with the assumption that the nonlinear problem solution is constant and is M = 1 for the concerned influence mode. It will be emphasized that in the non-stationary problems it is not known a priori, whether the vaporization with M = 1 takes place, or M is always less than one.

5.2 *Vaporization kinetics in plasma formation in vapors* [124–126]

With values of the intensity G sufficient for ionization of evaporated particles the vaporization conditions change qualitatively. The vaporization kinetics takes

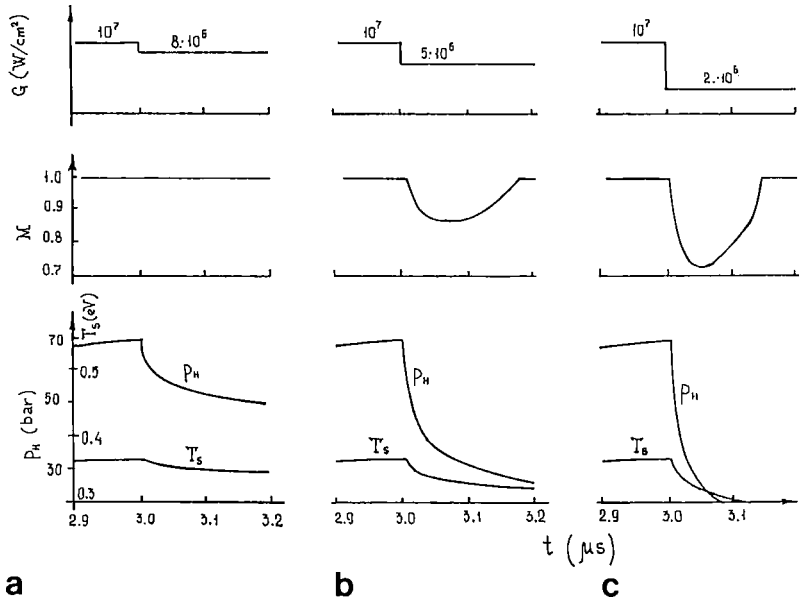

Fig. 15

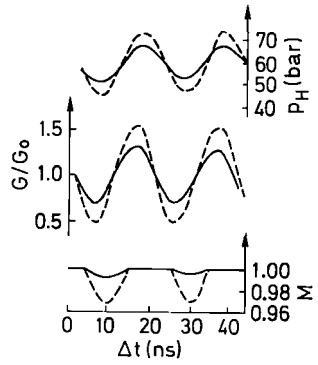

Fig. 16

a more complex nature, which is determined by two factors: temperature and gas-dynamics. The temperature factor comes into play because of the change of laser pulse intensity. The gas-dynamics factor is due to pressure variations, caused by a complex mechanism of substance separation in plasma formation. Ionization of vapors makes the gas opaque to laser radiation and an increasingly lesser part of it, being absorbed in the substance vapors, reaches the target surface. But simultaneously with the decrease of laser flow on the surface an increase of energy radiation flux occurs, coming out of plasma. Plasma formation leads to that situation even with a constant source G intensity of the flux, impinging upon the surface since the sum $G_s + W_s$ changes in a rather broad range of values, owing to variable optical transparence. In this way non-stationary conditions are produced on the surface. Partial laser radiation absorption by ionized vapors produces a sharp increase of pressure in the gas to values comparable with saturation pressure, thus causing an additional retardation of vapor flow and a decrease of the value of the parameter M.

From the mathematical point of view and for the one-space-dimensional case the processes discussed above can be described by the following system of equations:

$$\rho(T)C_p(T)\left(\frac{\partial T}{\partial t} - v_{lv}\frac{\partial T}{\partial x}\right) = \frac{\partial}{\partial x}\left(\lambda(T)\frac{\partial T}{\partial x}\right) \tag{5.3}$$

$$-H < x < 0$$

$$x = -H\colon\ \lambda\frac{\partial T}{\partial x} = 0$$

$$x = 0\colon\ \lambda(T)\frac{\partial T}{\partial x} = G_s + W_s - L_v\rho_l v_{lv}$$

$$G_s = (1 - R)G_0^+,\ G_0^- = (1 + R(T_s))G_0^+$$

$$\rho_s v_{lv} = \rho_0(u_0 - v_{lv}) \tag{5.4}$$

$$P_s + \rho_s v_{lv}^2 = p_0 + \rho_0 (u_0 - v_{lv})^2$$

$$T_0 = T_s \cdot \left\{ \left[1 + f^2 \cdot \left(\frac{\gamma - 1}{\gamma + 1} \right) \cdot \mathrm{M}^2 \right]^{1/2} - f \cdot \left(\frac{\gamma - 1}{\gamma + 1} \right) \cdot \mathrm{M} \right\}^2$$

$$\rho_0 = \frac{1}{2} \rho_H \left\{ \left(\frac{T_s}{T_0} \right)^{1/2} \cdot \left[(\gamma \mathrm{M}^2 + 1) \exp(b^2 \mathrm{M}^2) \operatorname{erfc}(b\mathrm{M}) - \frac{4f}{\pi} \mathrm{M} \right] + \frac{T_s}{T} \left[1 - 2 \cdot f \cdot \mathrm{M} \exp(b^2 \mathrm{M}^2) \operatorname{erfc}(b\mathrm{M}) \right] \right\}$$

$$\frac{\partial \rho}{\partial t} + \frac{\partial}{\partial x} (\rho (u - v_{lv})) = 0 \tag{5.5}$$

$$\frac{\partial (\rho u)}{\partial t} + \frac{\partial}{\partial x} \left(\rho \frac{(u - v_{lv})^2}{2} \right) = - \frac{\partial P}{\partial x} \tag{5.6}$$

$$\frac{\partial [\rho (\varepsilon + u^2/2)]}{\partial t} + \frac{\partial}{\partial x} \left[\rho \left(\varepsilon + \frac{(u - v_{lv})^2}{2} \right) \right] = - \frac{\partial (Pu)}{\partial x} - \frac{\partial W}{\partial x} - \frac{\partial G_g}{\partial x} \tag{5.7}$$

$$\mu \frac{\mathrm{d}I}{\mathrm{d}X} + \kappa_\nu I_\nu = \kappa_\nu I_{\nu p}, \quad W = \int_0^\infty \mathrm{d}\nu \int_{-1}^{1} \mu I_\nu \mathrm{d}\mu, \tag{5.8}$$

$$\frac{\mathrm{d}G^-}{\mathrm{d}x} + \kappa_\nu G^- = 0, \quad \frac{\mathrm{d}G^+}{\mathrm{d}x} - \kappa_\nu G^+ = 0, \quad G_g = G^- + G^+. \tag{5.9}$$

$$0 < x \leq L.$$

$$x = L: \quad P = 0, \quad G^+ = G, \quad I_\nu = 0 \tag{5.10}$$

Equation (5.3) describes the behavior of the condensed medium, (5.5) and (5.6) describes gas-dynamics equations, (5.7) is the equation of energy balance in gas medium, (5.8) and (5.9) are the equations of continuous and laser radiation, respectively.

Indices s, l and o are related to the surface of the condensed medium, liquid and external side of Knudsen layer, respectively.

W is an average radiation flux, $I_{\nu p}$ is an intensity of equilibrium radiation, W_s is radiation flux, being absorbed by the condensed medium surface.

Note, that the system of radiation gas-dynamics equations is written assuming the existence of local thermodynamical equilibrium in the gas.

The mathematical model of aluminum surface vaporization in vacuum by laser radiation with $\lambda = 1.06$ μm and $G = G_0 \exp(-2(\tau - t)^2/\tau^2)$, $G_0 = 5 \cdot 10^8$ W/cm^2, proposed in [124–126] according to (5.3)–(5.9) has shown that plasma formation causes not only a decrease of the evaporated substance flow, but, also, leads to a complete stopping of vaporization despite high surface temperature (Fig. 17). Under that condition parameter M takes negative values $\mathrm{M} < 0$ (Fig. 18). In the same figure the part of the evaporated substance flow $F = F_0/F_s$, having passed through the Knudsen layer, is shown. where $F_0 = \rho_0 u_0$ and $F_s = \rho_s v_{lv}$.

Formally, to $\mathrm{M} = 0$ it corresponds zero flow of substance over the interface. The condensation process must correspond to the negative values of M. The model

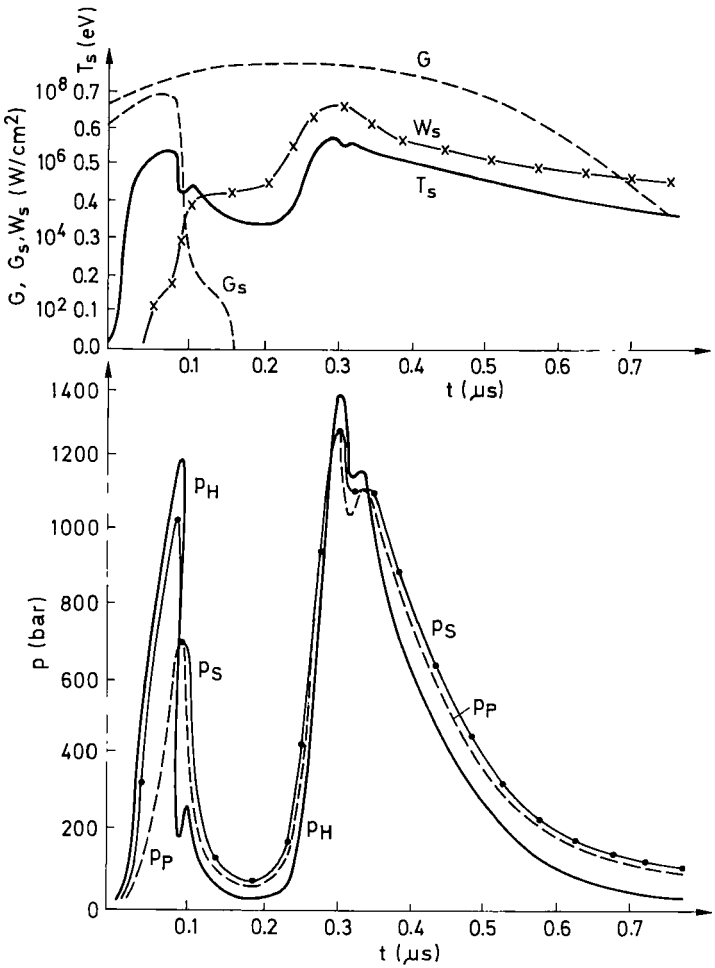

Fig. 17

(5.3)–(5.9) does not include the condensation kinetics, but it was believed that the whole flow of matter reaching the surface is deposited on it. From the curves in Fig. 18 it follows that vaporization occurs during two short time periods, where $M > 0$. The first vaporization period is caused by laser radiation and is characterized by the inequality $p_H > p_p$, where p_p is a pressure in plasma. As a result, $M > 0$. The plasma formation in vapors makes pressure increase to p_p and M decrease. The negative values of M are taken when $p_H < p_p$. The second period of vaporization is due to the flux of plasma intrinsic radiation W_s, the maximum value of which reaches $\sim 10\%$ of G. Note that during the second period vaporization occurs with a rate, significantly lower than the maximum one, $M \approx 0.1$. The appearance of a new portion of evaporated substance increases the optical thickness of plasma, which weakens the flux W_s and leads to the situation $p_H < p_p$, $M < 0$.

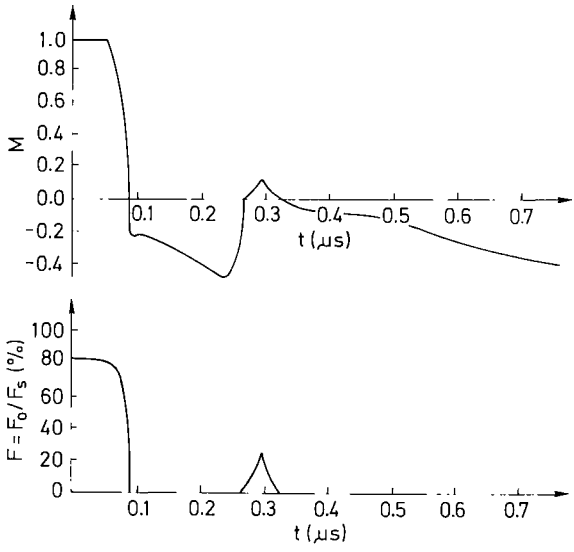

Fig. 18

A brief consideration of the main aspects of the problem of metal surface vaporization by laser radiation indicates an important role of gas-dynamics phenomena, even in vaporization into vacuum. This becomes more evident when we consider pressure controlled laser treatment of condensed substances. The vaporization of the substance can lead to the formation of impact waves and, depending on the chosen conditions, plasma will appear either in vapors, or in gas. Its composition and other characteristics will be considerably different from the ones of plasma formed during vaporization into vacuum.

Let us remark that the experimental and theoretical results available indicate that the studies of such processes are largely incomplete. At the same time, the optimization of such technological processes as laser cutting, welding, multilayer coatings, evaporation of superconducting ceramic films, i.e., of those processes in which phase transformations play a leading part, requires detailed information about the dynamics of all the processes taking place in the irradiation zone. But most problems in laser technology, still, can be solved only empirically.

In conclusion, we note that most of the theory here considered, in general, is applicable to laser miniature welding. The welding of large-size components, as a rule, performed by laser units under continuous or pulse-continuous conditions of radiations, must be described including also the hydrodynamical effects.

6 Laser-plasma treatment of metal

Laser-plasma treatment (LPT) is recognized as a whole complex of processes, in which laser plasma formed in gas under controlled pressure plays a significant role. Some tests [127, 128] have shown, that the presence of gas metals with a specified composition and a pressure controlled in the range 10–100 bar near the surface,

allows to change the laser radiation interaction with targets in a certain interval of intensity due to plasma formation, and to use laser plasma thermal-chemical properties in order to change the microhardness of metals. LPT of materials is a promising technological process, but its application for practical purposes is still at the initial stage.

We shall briefly describe the peculiarities of LPT in nitrogen, N_2, and carbon dioxide, CO_2, [1], atmospheres, for radiation with $\lambda_v = 1.06$ μm. Within the pressure range 1–40 bar plasma appears and develops, mainly, in vapors. With the increase of gas pressure up to 60 bar the significance of erosion processes reduces and under pressures exceeding 80 bar, plasma develops in the environmental gas. The influence of the chemically active medium, just laser plasma, promotes the formation of nitrides and carbides in the near surface layers of the material under treatment, with no substantial destruction by laser radiation. The formation of nitrides, carbides and other non-equilibrium structures in the radiation zone increases microhardness and wear resistance by 2–4 times for such metals as steel, titanium, molybdenum, tantalum, zirconium, and others [1, 128, 129]. It is not surprising, then, that the detailed analysis of the laws of laser plasma development and the study of its role in the general processes becomes very actual.

Conventionally the origin and development of laser plasma is divided into three successive stages: gas break-down, formation of plasma cloud opaque to laser radiation and quasi-stationary spread of plasma formations. The initial stages of development, in particular the stage of optical break-down, determining the subsequent nature of radiation interaction with the substance, are of major interest to us because they are less known than the third stage.

In study on the initial stages of the development it is necessary to consider the contribution of the processes both on the level of elementary collision reactions (excitation, ionization, deexcitation, recombination, dissociation, conversion of atoms and ions), and the influence of the macroscopic processes (diffusion, transfer, gas-dynamics separation). As the most part of collision reactions in the radiation zone proceeds under strong non-equilibrium conditions, the relation between the processes of chemical kinetics and gas dynamics can be of a very complex nature. Therefore, one should not rely too much on oversimplified models and on simple estimates. As we believe, a more promising way of studying such non-equilibrium systems is the development of sufficiently complete nonlinear mathematical models and realization of numerical experiments.

The optical break-down of gas has been the object of a comprehensive study for a long time [130–134]. As it has been already mentioned, gas break-down by radiation is characterized by a large number of interrelated and interdependent processes with different space and time scales, and moreover, proceeding under strong non-equilibrium conditions. While the properties and the state of a plasma in thermodynamic equilibrium are determined unambiguously by its temperature T and its density ρ, the determination of laser plasma properties and particularly its initial phase—optical break-down due to non-equilibrium—is a far more complex and difficult problem. In order to describe optical break-down, based on electron avalanche phenomenon, it is necessary to use the kinetic models, considering the processes of collision and radiation transitions in atoms, molecules, and ions.

6.1 Optical break-down
Kinetic models

The development of electron avalanche in vapors of metals can be described within the framework of the collision-radiational model [135], representing the system of equations of level kinetics, complemented by two equations of energy balance for the electron and atom-ion subsystems. The description of the level kinetics of atoms and ions is complicated by the fact that the energetic levels of the excited state are splitted and mixed between each other, which leads to the necessity of considering multiple transitions between them.

As an example, we will consider the collision-radiational model, describing the kinetics of the collision and radiation transitions in atoms and ions of Al and used for the study of the optical break-down of aluminum vapors [136]. The break-down conditions correspond to the intensive surface vaporization. As initial data the characteristic parameters of the evaporated substance on the external side of the Knudsen layer were specified. The electron configuration of aluminum atom $1s^2 2s^2 2p^6 3s^2 3p$ has three electrons with comparatively high ionization energy on the non-complete ionization shell: $I_1 = 5.986$ eV, $I_2 = 18.826$ eV, $I_3 = 28.348$ eV. For electrons of the complete shell the ionization energy is much higher than $I_4 = 120$ eV. Therefore, in the construction of the collision-radiational model only the neutral atom Al and the first two ions, Al^+ and Al^{++}, were considered. The ion Al^{+++} (Ne-like aluminum ion) was assumed to be structureless, i.e., a core. The excited states of neutral atom and two first ions considered, as well as the collision and radiation transitions between them, are given in Figs. 19–21. The level with the main quantum number $n = 6$ in the model was assumed to be hydrogen like, and the levels with $n > 10$ were combined as a ionization continuum. The level kinetics, charge content and energy balance in the given approach were described by the system of ordinary differential equations:

$$\begin{aligned}
&\frac{\partial N_i}{\partial t} = R_i + S_i - A_i;\ i = 1, \ldots, 11\\
&\frac{\partial N_i^{+}}{\partial t} = R_i^{+} + S_i^{+} - A_i^{+};\ i = 1, \ldots, 11\\
&\frac{\partial N_i^{++}}{\partial t} = R_i^{++} + S_i^{++} - A_i^{++};\ i = 1, \ldots, 11\\
&\frac{\partial N_i^{+++}}{\partial t} = \sum_i S_i^{++};\ i = 1, \ldots, 11
\end{aligned} \tag{6.1}$$

$$\begin{aligned}
\frac{\partial}{\partial t}\left[\frac{3}{2} N_e T_e\right] &= \left\{G\mu - 3\frac{M_a}{m_e}(T_e - T_g)\right\}(\nu_{en} + \nu_{ei})\\
&\quad + \sum_{i=1}^{11} (Q_i^{+} + Q_i^{++} + Q_i^{+++} + \tilde{Q}_i^{+} + \tilde{Q}_i^{++} + \tilde{Q}_i^{+++})\\
\frac{\partial}{\partial t}\left[\frac{3}{2} N_g T_g\right] &= 3\frac{M_a}{m_e}(T_e - T_g)(\nu_{en} + \nu_{ei}) N_e
\end{aligned} \tag{6.2}$$

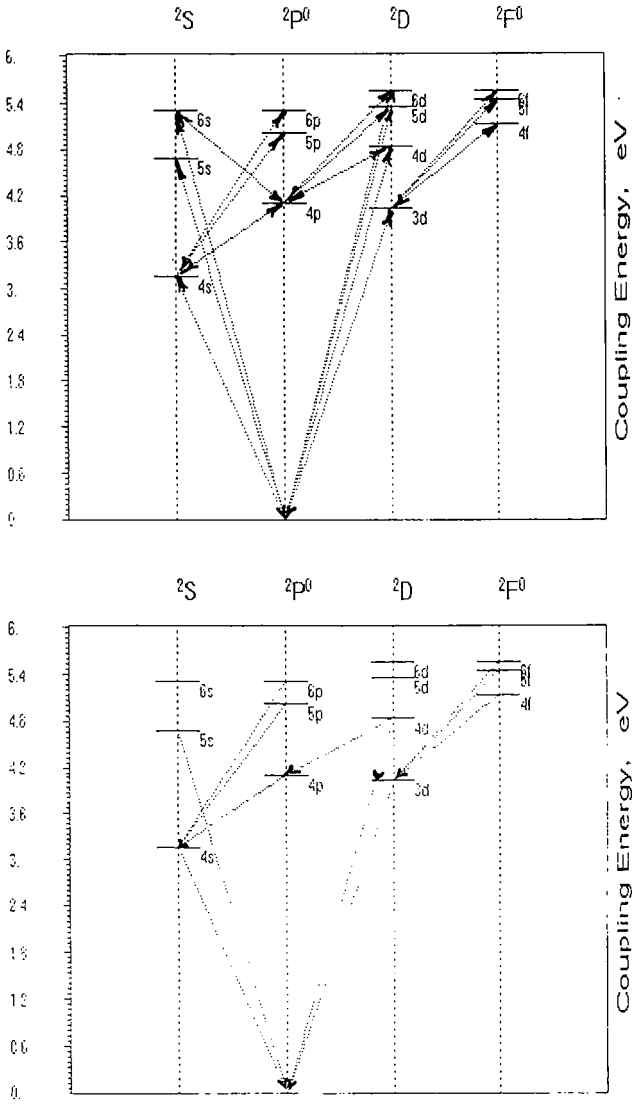

Fig. 19

where i, j are energy levels numbers, z is the particle type index (neutral atom or 1, 2, 3 times ionized atom); N_i^z, ΔE_{ij}^z are i-level population for z particle and difference between i-state binding energy and j-state binding energy for z particle; T_e, T_g denote electron and heavy particles temperatures; M_a, N_e, N_g, G_z, R_i^z are referring to aluminum atom mass, overall density of neutral atoms and ions, incident wave intensity, and i-state population rate of change for z particle because of collision transition, respectively.

$$R_i^z = N_e \sum_{j \in \Omega_i} (k_{ij}^z N_j^z - k_{ij}^z N_i^z),$$

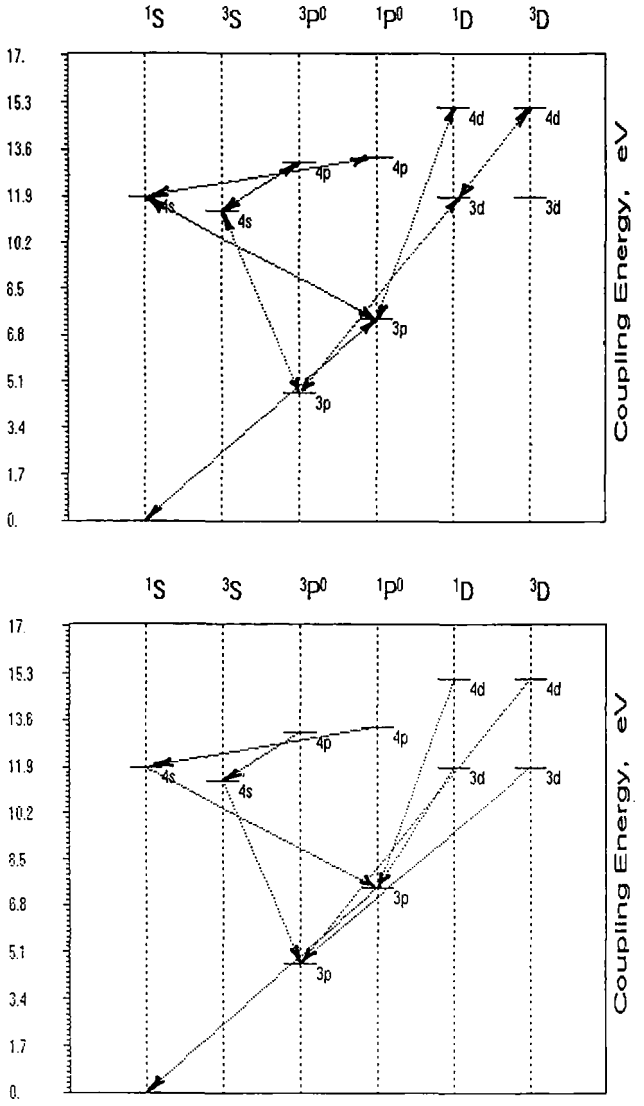

Fig. 20

where the summation set Ω_i consists of states numbers, transition from which to i-th states are allowed. S_i^z is the term which defines i-state population rate of change for z particle because of electron collision ionization process and three-particle recombination.

$$S_i^z = (\beta_i^z N_e N^{z+1} - \alpha_i^z N_i^z) N_e.$$

A_i^z is the i-state population rate of change for z particle because of spontaneous decay

$$A_i^z = a_i^z N_i^z.$$

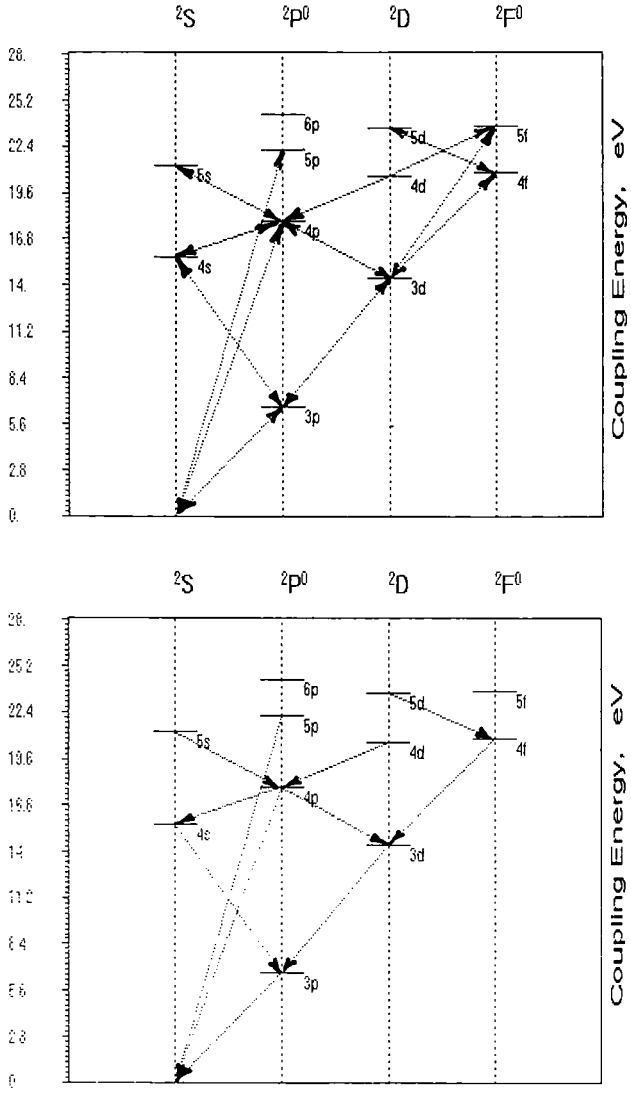

Fig. 21

Terms Q_i^z, $\tilde{Q}_i^z$ take into account the energy exchange between electron and 'heavy' component because of non-elastic exciting reactions, quenching, ionization and recombination:

$$Q_i^z = \sum_{j \in \Omega} |\Delta E_{ij}^z| (k_{ji}^z N_j^z - k_{ij}^z N_i^z) N_e$$

$$Q_i^z = (I^z - \Delta E_i^z)(\beta_i^z N_i^z N_e - \alpha_i^z N^{z+1}),$$

$$N^{z+1} = \sum^{11} N_i^{z+1}.$$

ν_{ei}, ν_{en} are the elastic electron-ion and electron-neutral collisions frequencies, respectively.

$$\nu_{ei} = \frac{3.6 \cdot 10^{-5}}{T_e^{3/2}} \sum_{j=1}^{11} [N_j^+ + N_j^{++} + N_j^{+++}],$$

$$\nu_{en} = \nabla_e \sigma_y \sum_{j=1}^{11} N_j = 2.2 \cdot 10^{-8} \sum_{j=1}^{11} N_j,$$

where $\nabla_e (= 6.7 \cdot 10^7 T_e^{1/2})$ is the mean velocity of electron heat motion, and $\sigma_y (= 3 \cdot 10^{-15}/T_e^{1/2})$ is the elastic collision cross-section.

μ is a parameter which defines the electron energy increase because of inverse brake effect (for one single collision):

$$\mu = \frac{4\pi e^2}{m_e C(\omega^2 + \nu^2)}, \quad \nu = \nu_{en} + \nu_{ei}.$$

Ion electron concentrations derived from (6.1)–(6.2) were compared to equilibrium values, deduced with the use of Sacha nonlinear equation system with temperature T_r, $r = e, g$:

$$\frac{N_e N_r^+}{N} = \frac{g_e \Sigma_r^+}{\Sigma} \left(\frac{m_e T_r}{2\pi}\right)^{3/2} \exp\left(-\frac{I}{T_r}\right),$$

$$\frac{N_e N_r^{++}}{N_r^+} = \frac{g_e \Sigma_r^{++}}{\Sigma_r^+} \left(\frac{m_e T_r}{2\pi}\right)^{3/2} \exp\left(-\frac{I^+}{T_r}\right), \tag{6.3}$$

$$\frac{N_e N_r^{+++}}{N_r^{++}} = \frac{g_e \Sigma_r^{+++}}{\Sigma_r^{++}} \left(\frac{m_e T_r}{2\pi}\right)^{3/2} \exp\left(-\frac{I^{++}}{T_r}\right),$$

where Σ, Σ_r are atom and ion static sums, respectively. I is the particle ionization energy.

The mathematical modeling has shown that the optical break-down of metal vapors represents a strong non-equilibrium transition state from partially ionized vapor, in which the Coulomb collisions frequency ν_{ei} is less than ν_{en}, to a strongly or completely ionized plasma, in which the Coulomb collisions frequency becomes dominant, $\nu_{ei} \gg \nu_{en}$ (Fig. 22). The non-equilibrium of the process is determined by the energy dissipation of laser radiation by the electron component, which leads to a considerable separation of temperature T_e from temperature T_g, $T_e > T_g$ (Fig. 23), disappearing only in the complete ionization region. The occurrence of this effect does not depend on whether the partially ionized vapor at the initial time is at the thermodynamical equilibrium or not.

The optical break-down is based on the cascade ionization having an avalanche-like development. In Fig. 24, the variation dynamics of the populations of the main (n^0) and excited (n^k) states of neutral atom is shown, by which one can get an idea of the nature of electron avalanche development. The comparison of the concentration of charge particles, calculated according to the kinetic model (6.1–6.2) and the Sacha equilibrium model (6.3), presents a great interest. Since there exists a significant difference between the electron temperature T_e and the temperature of heavy particles T_g, then the charge content is considerably different

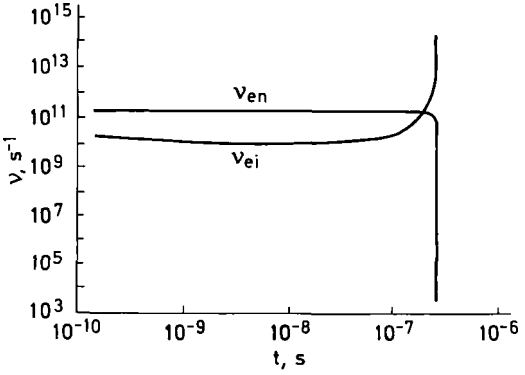

Fig. 22

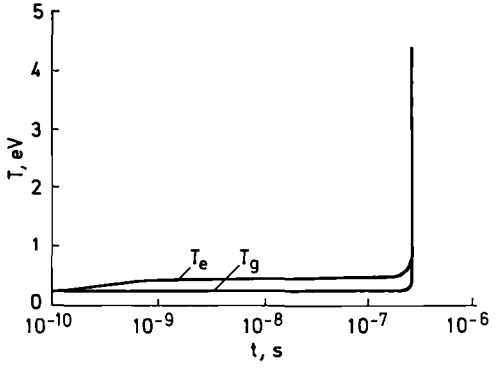

Fig. 23

from the one at equilibrium. In Fig. 25a–c, the time evolution of the charge particles concentration N_e, Al^+, Al^{++}, is presented, the non-equilibrium values are marked by solid lines. For comparison, the corresponding equilibrium values, calculated by Sacha equations (6.3), for two temperatures $T = T_e$ and $T = T_g$ are given (Fig. 25a–c, dotted lines). It is shown, that the values of the concentrations of N_e, Al^+, Al^{++}, calculated according to model (6.1–6.2), are between the equilibrium values, being significantly less than the values, taken when the medium temperature was assumed to be $T = T_e$, but being much larger than the equilibrium values with temperature $T = T_g$. As the temperatures T_g and T_e become closer, the non-equilibrium values of the concentrations N_e, Al^+, Al^{++} approach the non-equilibrium ones $N_e = N_e(T_e) = N_e(T_g)$, $Al^+ = Al^+(T_e) = Al^+(T_g)$, $Al^{++} = Al^{++}(T_e) = Al^{++}(T_g)$.

With respect to radiation intensity the optical break-down is of a sharply pronounced threshold nature. The threshold value of intensity in many respects depends on the initial data: temperature, density and medium ionization extent (Fig. 26).

The description of electron avalanche development in atomic gases, can be made within the framework of simpler mathematical models. For most atomic gases the cascade ionization with a sufficient accuracy degree can be described with the account of resonance excitation level only [137, 138].

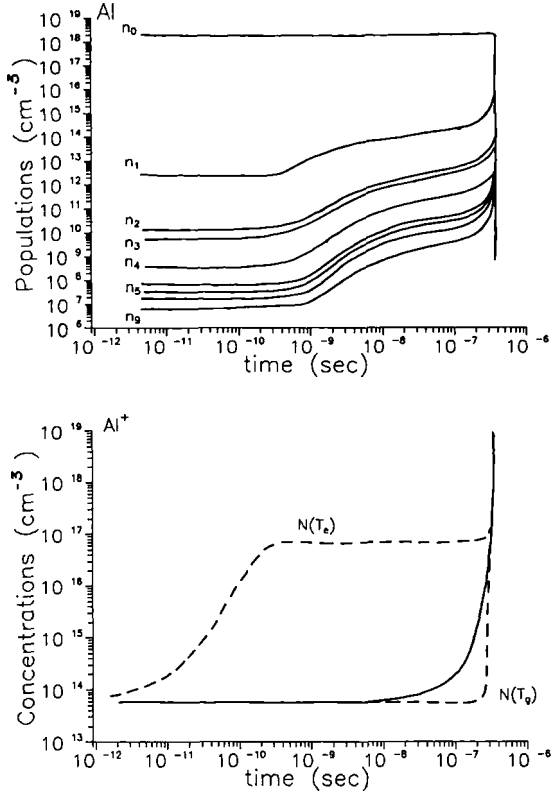

Fig. 24

The electron avalanche description in molecular gases is significantly complicated by the existence of rotation and oscillation degrees of freedom, which requires the consideration of numerous rotation and oscillation levels. In papers [139, 140] a kinetic model for molecular nitrogen, further used for the optical break-down modeling near the metal surface at increased gas pressures, has been proposed. The mathematical model was written in one-space-dimensional and three temperatures approach (two forward temperatures for electron and heavy particles and one oscillation temperature for molecules). The calculations have shown that in the region of moderate intensities $G < 10^9$ W/cm^2 one of the channels for the optical break-down of molecular gas development is the almost complete dissociation of molecules, so that the electron avalanche then develops in the atomic component.

6.2 Laser plasma dynamics
Radiation gas-dynamics models

The determination of the main characteristics of the break-down allows to turn to simulation of the next stage of laser plasma development, in which the macroscopic motion and the related energy balance and, in particular, radiation transfer, play the principal role. After the optical break-down from the ignition region towards

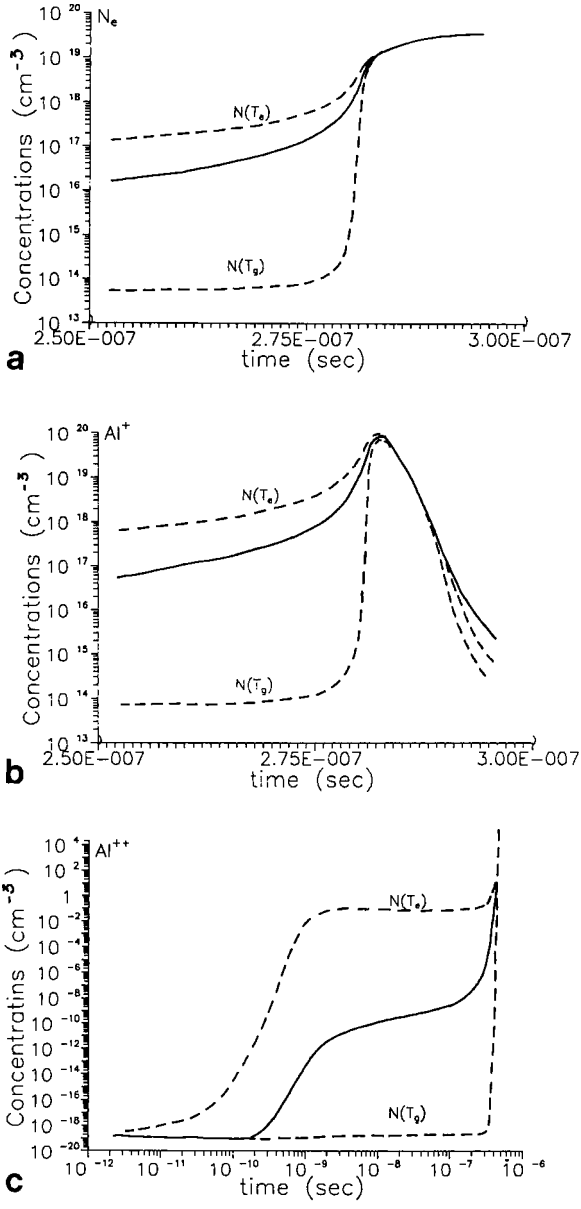

Fig. 25

laser radiation, the absorption wave moves, leaving behind it plasma formations, for which we can believe that the conditions of local thermodynamical equilibrium are fulfilled. The evolution of the laser plasma gas-dynamics stage in nitrogen under increased pressure attracts attention, first of all, for the fact that at this stage alongside with the laser radiation influence the interaction of laser plasma formation with the target surface takes place. The nature of the interaction, as the

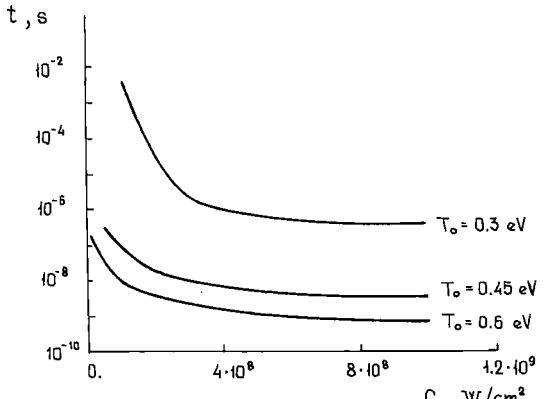

Fig. 26

calculations have shown [136–138], depends to a considerable extent on such laser plasma parameters as geometrical sizes, temperature, density of ions and radiation fluxes from plasma to the target. One of the most important conditions of the treatment, which determine the thickness of the metal synthesized layer, is the requirement of maximum duration of the contact of nitrogen plasma with the surface.

The peculiarity of the processes we are considering is that at high pressures besides the hydrodynamical mechanism of energy transfer, the radiation transfer plays a significant role. On the contrary, heat conduction is not essential. Moreover, under conditions of laser pulse high duration $\tau \sim 10^{-3}$ s and a relatively small focusing spot $d \sim 500$ μm the effects of two-dimensionality, arising because of the radial extension of plasma cloud, appear to be essential.

The main characteristics and spreading mechanism of low-temperature laser plasma, being developed near the metal surface in nitrogen under pressure $p = 10^2$ bar and radiation $G = 10^7$–10^8 W/cm^2 with $\lambda_v = 1.06$ μm were studied in papers [141–143] by mathematical modeling of two-dimensional problems in radiational gas-dynamics. The system of two-dimensional axial-symmetric equations of radiation gas dynamics, written in Lagrange variables was used for simulation:

$$\frac{d\rho}{dt} = -\rho\left(\frac{1}{r}\frac{\partial(ru)}{\partial r} + \frac{\partial v}{\partial z}\right)$$

$$\rho\frac{du}{dt} = -\frac{\partial(p+\omega)}{\partial r}, \quad \rho\frac{dv}{dt} = -\frac{\partial(p+\omega)}{\partial z}$$

$$\rho\frac{d\varepsilon}{dt} = -p\left(\frac{1}{r}\frac{\partial(ru)}{\partial r} + \frac{\partial r}{\partial z}\right) - \frac{1}{r}\frac{\partial(rW_r)}{\partial r} - \frac{\partial W_z}{\partial z} - \frac{\partial G}{\partial z}$$

$$\frac{1}{r}\frac{\partial(rW_r^k)}{\partial r} + \frac{\partial W_z^k}{\partial z} + \kappa U_k = \kappa_k U_{kp} \tag{6.4}$$

$$\frac{1}{3}\frac{\partial U_k}{\partial r} = -\kappa_k W_r^k, \quad \frac{1}{3}\frac{\partial U_k}{\partial z} = -{}_k\kappa W_z^k, \quad W = \sum_{k=1}^{N} W^k$$

$$p = p(T, \rho), \quad \varepsilon = \varepsilon(T, \rho), \quad \kappa = \kappa(T, \rho, \nu)$$

where r, z are space coordinates, t is time, ρ, p, and ε are density, pressure, and internal energy, κ_k is the photon absorption coefficient of frequency $\nu \in [\nu_k, \nu_{k+1}]$, W is an average radiation flux, U, U_p are radiation density and radiation equilibrium density, G is the laser radiation intensity, w is the artificial viscosity, n is the number of groups. The radiation transfer process was described in many groups approach ($N = 7$). The break-down stage was simulated according to the data about the optical break-down [139, 140] specifying the hot region with 15–20 μm thickness and temperature (expressed via an equivalent thermal energy) $T = 1.5$–1.8 eV.

The calculations have shown that the threshold value of the intensity required for keeping laser plasma development in the pressure range of 30–100 bar, is $G = 4.4 \cdot 10^7$ W/cm^2. In Figs. 27 and 28 the space-time profiles of plasmoid section for pressure 100 bar (Fig. 27) and 30 bar (Fig. 28) are shown. In these problems laser radiation is incident along axis z and is intensively absorbed in the hot region, followed by the appearance and spreading of the shock wave to cold gas. The regions enveloped in the shock wave are emphasized in the figures by dotted lines and characterized by the jump of density ρ and pressure p. The maximum velocity of the shock wave reaches ~ 1.5 km/s, its temperature is ≤ 0.35 eV. At such

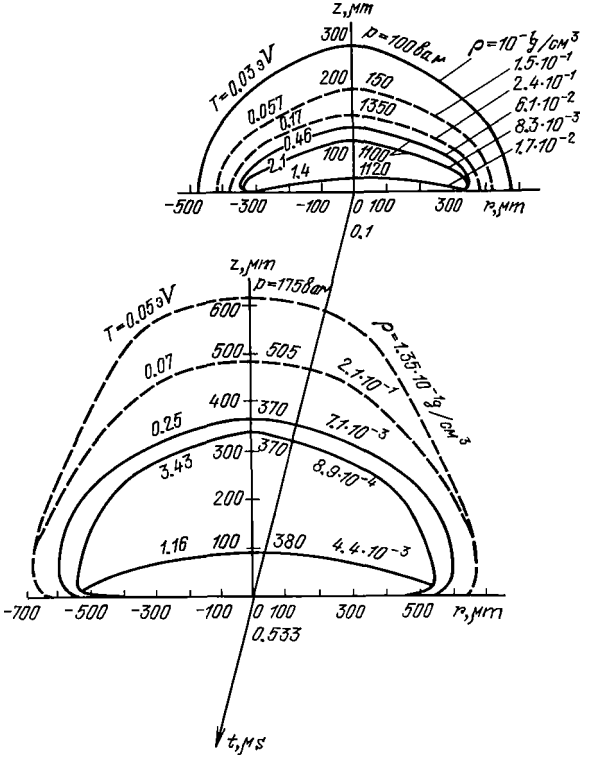

Fig. 27

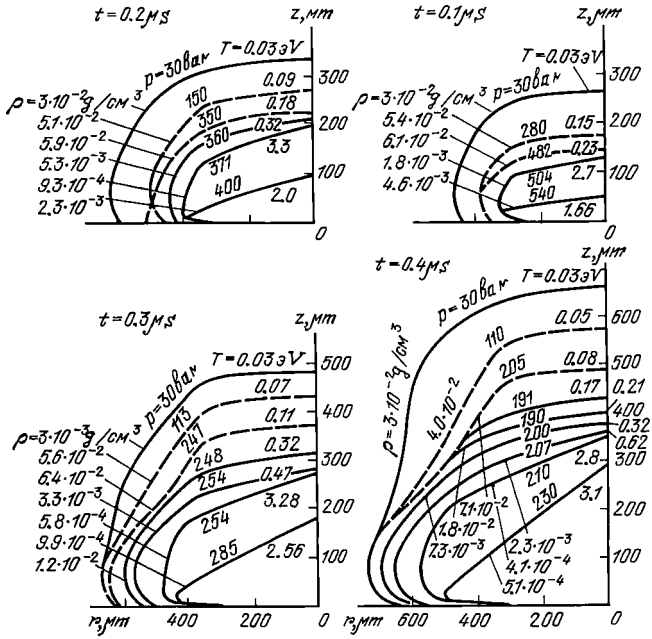

Fig. 28

temperature the impact wave is transparent to laser radiation. The shock wave velocity significantly exceeds the velocity of the plasma front and, as a result, the shock wave becomes separated from the hot region and decays. The plasmoid has a complex structure. For example at $p = 100$ bar the temperature of the surface layer ($T \approx 1$ eV) is essentially lower than the temperature of lower located layers, where $T \approx 3.5$ eV. The explanation of this phenomenon is related to the screening of laser radiation and to two-dimensional laser separation of the hot region. As a result, the surface is affected only by the flux of plasma intrinsic radiation W, whose value does not exceed $5 \cdot 10^5$ W/cm^2. The area, subject to the thermal influence of radiation fluxes, is several times higher than the one of the focusing spot. Lowering laser radiation flux by 2.5 orders, is the main protection against surface failure. In the test [127, 128] a decrease of external pressure to 30–50 bar led to the target surface failure, manifested in the form of craters in the region of influence. The simulation has shown that if pressure is kept at $p = 30$ bar for $t \leq 0.1$ μs the process develops in the same manner as at 100 bar. Laser radiation is absorbed in the hot region, a complex region with different temperatures is formed in every layer. The radiation flux reaches a value of $3 \cdot 10^8$ W/cm^2, and the region of influence has a radius ~ 600 μm. Furthermore, the nature of the interaction of radiation with the substance changes. Due to a lower initial density of the substance at $p = 30$ bar, the intensive separation of plasma make plasma transparent to laser radiation at $t \approx 0.5$ μs. In Fig. 29, the time evolution of laser intensity $G(t)$ and radiation flux $W(t)$, reaching the surface and determining its thermal conditions, are presented. From the non-monotonicity of $G(t)$ it follows that at

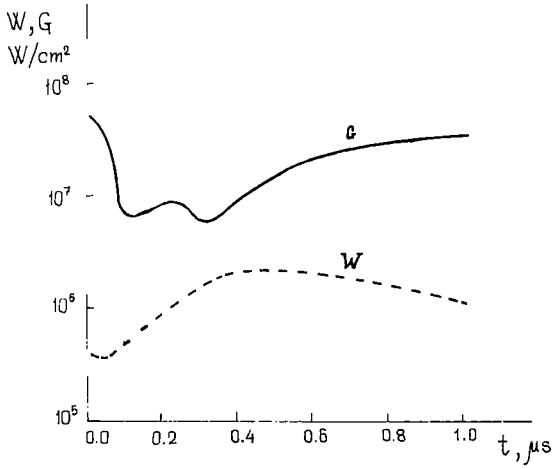

Fig. 29

$t = 0.1$–0.4 μs the flux on the surface is significantly reduced due to absorption in the poorly transparent plasmoid, but by $t \approx 1$ μs because of the plasma brightening caused by surface detachment it achieves $\sim 80\%$ of laser radiation.

The reduction of screening triggers an intensive vaporization of the surface. The persistence for some time of a plasma cloud of low transparency to laser radiation can be exploited for optimizing treatment conditions. Such optimization has been obtained by time modulation of the laser pulse [144]. At the moment of the highest absorption the intensity of laser radiation becomes several times smaller, and consequently the optical thickness of the plasma cloud is reduced. As a result, with the decrease of the working pressure to 30 bar an increase of the contact time of the hottest layers of plasma with the surface and consequently an increase of the synthesized surface layer thickness was successfully achieved.

In conclusion, we note that in this field of research the main problems of mathematical modeling are concerned on one side with phenomena of non-equilibrium radiation gas-dynamics, and their connections with the behavior of the condensed medium, and on the other side with the development of appropriate numerical algorithms for the computation of the solutions. Presently the authors work on these problems.

7 Automation of calculations

All the conclusions about the main aspects of laser influence on materials indicate mathematical modeling as a fundamental tool in the study and for the determination of the treatment optimum conditions. At the same time thermodynamical and hydrodynamical processes, following the radiation influence, have not been studied to such an extent that in most cases the engineering calculations can be made to determine the main characteristic quantities, such as temperature gradients and velocities of phase interfaces with accuracy within 5–10%.

The existence in the problem under consideration of such poorly controlled factors as the space-time fluctuations of laser pulse intensity and the fluctuations of the surface absorptivity implies the necessity of carrying out large series of calculations with a set of parameters changing over a broad range of values. The question about the automation of calculation, which can be performed with the help of compact highly efficient program packages, becomes actual.

We are creating a family of the programs under the general title LASTEC, designed for the simulation of different conditions of laser influence on metals, dielectrics and semiconductors. At present the first two packages LASTEC-1 and LASTEC-2 have been completed [145, 146].

The mathematical basis of both packages is a one-dimensional non-stationary Stefan problem for multiphase regions. LASTEC-1 takes into account the processes of simultaneous melting and vaporization in homogeneous materials with a surface (metals) and bulk (dielectrics, semiconductors) energy source. LASTEC-2 has been created for studies on similar processes in the multi-layer structures with an ideal thermal contact on the boundaries. The maximum number of materials permissible in the structure is four. The high computation efficiency of the numerical algorithms in both packages is achieved by the application of finite-difference schemes with dynamically adapted calculation grids [60–63]. The use of dynamically adapted grids allows to identify the phase boundaries in an obvious way and to use a homogeneous computational algorithm.

The packages LASTEC-1, LASTEC-2 are designed for simulation of the processes, in which the phase transition of 1st type plays a significant role. With their help the temperature fields in the bulk, the phase boundaries velocities, the heating and cooling rates of the sample, the depth of the melting and evaporated layers, both in homogeneous and in heterogeneous media, can be efficiently determined. The packages are orientated to PC-AT 386, 486 personal computers and can be used as a technological line component with the help of which an engineer-technologist can choose the optimum values of intensity and influence duration. Such a choice can be made also in the case when reliable data about the material to be treated are unavailable. For these purposes the packages are conceived in a flexible way, so that the user can introduce any law of absorptivity, heat conduction coefficients, and thermal capacity. Also, comparison of numerical results with experimental data can help to determine the most reliable and optimum conditions for treatment.

8 Conclusion

Certainly, the whole problem of mathematical modeling of laser influence in the technological range of radiation intensity is not reduced to the questions we have considered in this paper. Many interesting and important aspects of this problem are only sketched, and others were not touched upon at all (for instance, the influence of hydrodynamical effect and so on). A voluminous literature in the form of original papers, reviews, and monographs is dedicated to laser radiation influence on absorbing media.

Our aim was to attract attention of the specialists to the fact that the potential possibilities of laser technologies in metal treatment, machine building, and

microelectronic industry are extremely high. At the same time, from the point of view of an engineer-technologist, a laser influence contains a number of not yet understood effects, essentially influencing the technological process. In this connection additional studies are necessary, for which mathematical modeling is a support of decisive importance.

Acknowledgement

The authors express their sincere thanks to the referee for the detailed reports which greatly improved the presentation of the material.

References

1. Rykalin, N.N., Uglov, A.A., Zuev, I.V., Kokora, A.N.: Laser and electron-beam treatment of materials. Mashinostroenie, Moscow (1985).
2. Samarskii, A.A.: Theory of finite difference schemes. Nauka, Moscow (1977).
3. Ready, J.F.: Effects of high-power laser radiation. Academic Press, New York (1971).
4. European Scientific Laser Workshop on Mathematical Simulation, Lisbon, pp. 73–142 (1989).
5. Gurevich, L.O., Sobol, E.N.: Influence of diffusion limited α-γ-transformation kinetics upon calculation of hardened layer depth under laser heat treatment of steel. Izv. Akad. Nauk S.S.S.R. Met. 6: 154–158 (1984).
6. Basov, N.G. (ed.): Laser technology and investigation automation. Proc Lebedev Inst 198: 5–23 (1989).
7. Novikov, N.I.: Phase transitions in crystals. Inzh. Fiz. Zh. 39: 1118–1132 (1980).
8. Carslaw, H.S., Jaeger, J.G.: Conduction of heat in solids. Clarendon, Oxford (1959).
9. Oleinic, O.A.: About one method of Stefan-like problem solution. Dokl. Akad. Nauk S.S.S.R. 135: 1054–1057 (1960).
10. Kamenomostskaya, S.L.: About Stefan problem. Mat. Sb. 53: 488–514 (1961).
11. Friedman, A.: One dimensional Stefan problem with nonmonotone free boundary. Trans. Amer. Math. Soc. 133: 89–114 (1968).
12. Duvaut, G.: Resolution d'un probleme de Stefan. C.R. Acad. Sci. Paris 276A: 1461–1463 (1973)
13. Friedman, A., Kinderlehrer, D.: A one phase Stefan problem. Indiana Univ. Math. J. 24: 1005–1035 (1975).
14. Caffarelli, L.A.: Some aspects of the one-phase Stefan problem. Indiana Univ. Math. J. 27: 156–184 (1978).
15. Meyrmanov, A.M.: Nonexistence example of the classic solution of Stefan problem. Dokl. Akad. Nauk S.S.S.R. 258: 547–549 (1981).
16. Primicerio, M.: Mushy region in phase-change problem. In: Gorenflo, R., Hoffman, K. H. (eds.): Applied nonlinear functional analysis. Lang, Frankfurt/Main, pp. 251–296 (1982).
17. Fasano, A., Primicerio, M.: General free boundary problems for the heat equation I, II, III. J. Math. Anal. Appl. 57: 694–723 (1977); 58: 202–231 (1977); 59: 1–14 (1977).
18. Dowden, J., Kapadia P.: J. Phys. D. 22: 741–749 (1989); 21: 1255–1260 (1988).
19. Cryer, C.W.: A bibliography of free boundary problem. University of Wisconsin, Madison, Math. Res. Center, Tech. Summary, Report no. 1793 (1977).
20. Magenes, E.: Problemi di Stefan bifase in piu variabili spaziali. Matematiche 36: 65–108 (1983).
21. Nitsche, J.A.: A finite element method for parabolic free boundary problems In: Free boundary problems. Proceedings of the Seminar in Pavia. Istituto Nazionale di Alta Matematica, Rome, pp. 277–318 (1980).
22. Tarzia, D.A:. Una revision sobre problemas de frontera movil y libre para la ecuacion del calor. El problema de Stefan. Universidad Nacional de Rosario, 19: 147–241
23. Niezgodka, M.: Stefan-like problems. In: Fasano, A., Primicerio, M. (eds.): Free boundary problems: theory and application. Wiley, New York, pp. 321–348 (Research Notes in Mathematics, vol. 79) (1983).
24. Daniluk, I.I.: About Stefan problem. Usp. Mat. Nauk 40: 133–185 (1985).
25. Meyrmanov, A.M.: Stefan problem. Nauka. Novosibirsk (1986).
26. Crank, J.: Free and moving boundary problems. Clarendon, Oxford (1984).

27. Elliott, C.M., Ockendon, J.R.: Weak and variational methods for moving boundary problems. Wiley, New York Research Notes in Mathematics, vol. 59 (1982).
28. Friedman, A.: Variational principles and free boundary problems. Wiley, New York (1982).
29. Atthey, D.R.: A finite difference scheme for melting problems. J. Inst. Math. Appl. 13: 353–366 (1974).
30. Samarskii, A.A., Moiseenko, G.D.: Effective homogeneous scheme for multi dimensional Stefan problem. Zh. Vychisl. Mat. Mat. Fiz. 5: 816–827 (1965).
31. Vasiliev, F.P.: About finite difference method for the solution of homogeneous Stefan problem. Zh. Vychisl. Mat. Mat. Fiz. 3: 861–873 (1963).
32. Bachelis, R., Melamed, V., Shlaifer, D.: The solution of the problem of Stefan type by the straight line method. Zh. Vychisl. Mat. Mat. Fiz. 9: 585–594 (1969).
33. Davis, M., Kapadia, P., Dowden J.: Solution of a Stefan problem in the theory of laser welding by the method of lines. J. Comput. Phys. 60: 534–548 (1985).
34. Uspensky, A.B.: About front-flattening method for multi-frontal one dimensional Stefan-like problem. Dokl. Akad. Nauk S.S.S.R. 172: 61–64 (1967).
35. Hastaoglu, M.A.: Numerical solution to moving boundary problem- -application to melting and solidification. Int. J. Heat Mass Transfer 29: 495–499 (1986).
36. Crank, J., Gupta: Isotherm migration method in two dimensions. Brunel University Tech. Rep. 42 (1974).
37. Meyer, G.H.: The numerical solution of Stefan problems with front-tracking and smoothing methods. Appl. Math. Comput. 4: 283–306 (1978).
38. White, B.R.E.: A modified finite difference scheme for the Stefan problem. Math. Comput. 41: 816–827 (1983).
39. Biswajit Basu, Date, A.W.: Numerical modeling and solidification problems—a review. Sadhana 13: 169–213 (1988).
40. Mazhukin, V.I., Poveshchenko, Yu.A., Popov, Yu.P., Popov S.B.: Homogeneous algorithm of Stefan problem's numerical solution. Preprint IPM Im. M.V. Keldysha Akad. Nauk S.S.S.R. no. 122 (1985).
41. Meyer G.H.: Multidimensional Stefan problem. SIAM J. Numer. Anal. 10: 522–538 (1973).
42. Rogers, I.S.W., Berger, A.E., Ciment, M.: The alternating phase truncation method for solution of a Stefan problem. SIAM J. Numer. Anal. 16: 563–587 (1979).
43. Chen, J.C., Huang, Y.C.: Thermocapillary flows of surface melting due to a moving heat flux. Int. J. Heat Mass Transfer 34: 663–671 (1991).
44. Schneider, G.E.: Computation of solid/liquid phase change including free convection—comparison with data. J. Thermophys. 4: 366–373 (1990).
45. Ishiguro, H., Ohyama, K., Narial, H., Teramoto, T.: Numerical analysis of buoyancy and marangoni convection in melted zone of metals under high power laser irradiation. J. Nuclear Sci. Techn. 27: 1115–1125 (1990).
46. Schellhorn, M.: Transit thermocapillary flow induced by CO_2-laser heating. European Scientific Laser Workshop, Lisbon, pp. 161–177 (1989).
47. Voller, V.R., Brent, A.D., Prakash, C.: Modeling the mushy region in a binary alloy. Appl. Math. Model. 14: 320–326 (1990),
48. Lacroix, M., Voller, V.R.: Finite difference solution of solidification phase change problems: transformed versus fixed grids. Numer. Heat Transfer B 17: 25–41 (1990).
49. Lacroix, M., Garon, A.: Numerical solution of phase change problems: an Eulerian-Lagrangian approach. Numer. Heat Transfer B 19: 57–78 (1992).
50. Effect of laser radiation on absorbing condensed matter. Proceedings of the Institute of General Physics Academy of Sciences of the USSR, vol. 13, Nova Science, New York (1990).
51. Richtmyer, R.D., Morton, K.W.: Difference methods for initial-value problems. Interscience, New York (1967).
52. Samarskii, A.A., Popov, Yu. P.: Finite-difference methods of gas dynamics problems solution. Nauka, Moscow (1992).
53. Kristian, G.: Transformation theory in metal and alloys. Mir, Moscow (1978).
54. Koster, U., Herold, U.: Crystallization of glassy metals. In: Guntherodt, H.J., Beck, H. (eds.): Glassy metals I. Springer, Berlin Heidelberg New York, pp. 325–371 (1981).
55. Shklovsky, V.A.: Laser vitrification theory with phase transformation kinetics. Poverkhnost 6: 91–96 (1986).
56. Anisimov, S.I., Imas, Ya. A., Romanov, G.S., Khodyko, Yu. V.: High power radiation influence upon metals. Nauka, Moscow (1970).
57. Mazhukin, V.I., Samohin, A.A.: Mathematical modeling of phase transition and plasma formation under laser radiation influence on absorptive condensed substances. In: Samarskii, A.A. (ed.):

Mathematical modeling. Nonlinear differential equations of mathematical physics. Nauka, Moscow, pp. 191–244 (1987).
58. Masters, J.I.: Problem of intense surface heating of a slab accompanied by change of phase. J. Appl. Phys. 27: 477–484 (1956).
59. Knigt, C.J.: Theoretical modeling of rapid surface vaporization with back pressure. AIAA J. 17: 519–523 (1979).
60. Dar'in, N.A., Mazhukin, V.I.: Stefan problems numerical solution on adaptive grids. Dif. Uravneniya 23: 1154–1160 (1987).
61. Breslavsky, P.V., Mazhukin, V.I.: Mathematical modeling of processes of metal pulse melting and evaporation with explicit front-tracking. Inzh. Fiz. Zh. 57: 107–114 (1989).
62. Mazhukin, V.I.: Stefan problems mathematical modeling on adaptive grid. Heat/Mass Transfer--MIF, Materials of Minsk International Forum, pp. 125–139 (1988).
63. Dar'in, N.A., Mazhukin, V.I.: One approach to adaptive grids generation. Dokl. Akad. Nauk. S.S.S.R. 298: 64–68 (1988).
64. Vasilevsky, V.F., Mazhukin, V.I.: Numerical calculations of temperature waves with slight discontinuity on dynamically adaptive grid. Dif. Uravneniya 25: 1188–1193 (1989).
65. Mazhukin, V.I., Takoeva, L.Yu.: Generation principles for grids dynamically adaptive to solution in one-dimensional boundary problems. Mat. Modellirovaniye 2: 101–118 (1990).
66. Thompson, J.F., Warsi, Z.U., Mastin, C.W.: Boundary-fitted coordinate systems for numerical solution of partial differential equations- a review. J. Comput. Phys. 47: 1–108 (1982).
67. Brackbill, J.U., Saltzman, J.S.: Adaptive zoning for singular problems in two dimensions. J. Comput. Phys. 46: 342–368 (1982).
68. Thompson, J.F.: Grid generation technique in computational fluid dynamics. AIAA J. 3: 1505–1523 (1984).
69. Gclinas, R.J., Doss, S.K., Miller, K.: The moving finite element method: applications to general partial differential equations with multiple large gradients. J. Comput. Phys. 40: 202–249 (1981).
70. Dwyer, H.A.: Grid adaption for problems in fluid dynamics. AIAA J. 22: 1705–1712 (1984).
71. Bell, J.B., Shubin, G.R.: An adaptive grid finite difference method for conservation laws. J. Comput. Phys. 52: 569–591 (1983).
72. Anderson, D.A.: Equidistribution schemes, Poisson generation, and adaptive grids. Appl. Math. Comput. 24: 211–227 (1987).
73. Matsuno, K., Dwyer, H.: Adaptive methods for elliptic grid generation. J. Comput. Phys. 77: 40–52 (1987).
74. Verwer, J.G., Blom, J.G., Sanz-Serra, J.M.: An adaptive moving grid method or one-dimensional equations. J. Comput. Phys. 82: 454–486 (1989).
75. Nochetto, R.H., Paolini, M., Verdi, C.: An adaptive finite element method for two-phase Stefan problems in two space dimensions. Part 1. Math. Comput. 57: 73–108 (1991).
76. Nochetto, R.H., Paolini, M., Verdi, C.: An adaptive finite element method for two-phase Stefan problems in two space dimensions. Part 2: Implementation and numerical experiments. SIAM J. Sci. Statist. Comput. 125: 1207–1244 (1991).
77. Liseykin, V.D.: Technology of designing of 3-dimensional grids for aerodynamics problems. Vopr. Atom. Nauki Teh. Mat. Modellirovaniye 3: 31–45 (1991).
78. Wathen, A.J.: Optimal moving grids for time-dependent partial differential equations. J. Comput. Phys. 101: 51–54 (1991).
79. Breslavsky, P.V., Mazhukin, V.I., Takoeva, L.Yu.: Mathematical modeling of laser melting and evaporation of homogeneous materials. LASTEC-1 package. Preprint All-Union Center for Math. Modeling Est. S.S.R. Acad. Sci. no. 22 (1991).
80. Breslavsky, P.V., Mazhukin, V.I., Samokhin, A.A.: About hydrodynamical version Stefan problem for a substance at metastable state. Dokl. Akad. Nauk. S.S.S.R. 320: 1088–1092 (1991).
81. Gorelik, A.G., Dubinin, N.V., Mazhukin, V.I., Muzafarov, Kh.A.: Mechanism of polymers distraction by laser radiation. Preprint All-Union Center for Math. Modeling Est. S.S.R. Acad. Sci. no. 7 (1991).
82. Skripov, V.P., Koverda, V.P.: Spontan crystallization of under cooled liquid. Nauka, Moscow (1984).
83. Borodina, G.G., Kopetsky, I.V., Karposhin, V.S., et al.: Amorph structure formation from Fe-based alloys under the surface treatment by laser radiation. Dokl. Akad. Nauk S.S.S.R. 259: 826–829 (1981).
84. Karpov, S.Yu., Kovalchuk, Yu.V., Pogorelsky, Yu.V. : Semiconductor melting by pulse laser radiation. Phiz. Tek. Poluprovodnikov 20: 1945–1969 (1986).
85. Lees, J., Williamson, B.H.J.: Combined very high pressure/high temperature calibration of the tetrahedral anvil apparatus, fusion curves of zinc, aluminum, germanium and silicon to 60 kilobars. Nature (Physics) 208: 184–185 (1965).

86. Holian, K.S.: A new equation of state for aluminium. J. Appl. Phys. 59: 149–157 (1986).
87. Breslavsky, P.V., Mazhukin, V.I.: Computational algorithm of a hydrodynamical version of Stefan problem by dynamically adapting grid. Mat. Modellirovaniey 3: 104–115 (1991).
88. Dar'in, N.A., Mazhukin, V.I., Samarskii, A.A.: A finite-difference method of solving one-dimensional gas-dynamics equations on adaptive grids. Sov. Phys. Dokl. 302: 1078–1081 (1988).
89. Vasilevsky, V.F., Mazhukin, V.I.: Computation of shock waves on dynamically adaptive grids. Preprint of Keldysh Inst. Acad. Sci. U.S.S.R. no. 37 (1990).
90. Dar'in, N.A., Mazhukin, V.I., Smarskii, A.A.: Finite-differences method for solution of nonstationary two-dimensional problems on adaptive grid dynamically connected with solution. Preprint of Keldysh Institute Acad. Sci, U.S.S.R. no. 117 (1987).
91. Dar'in, N.A., Mazhukin, V.I.: Mathematical modeling of nonstationary two-dimensional boundary problem on dynamically adaptive grids. Mat. Modellirovaniye 1: 29–43 (1989).
92. Copley, S.M., Beck, D., Esquivel, O., Bass, M.: Laser melt quenching and alloying. In: Ferris, S.D., Leamy, H.J., Poate, J.M. (eds.): Laser-solid interaction and laser processing—1978. AIP Conference Proceedings no. 50. American Institute of Physics, New York, pp. 161–172 (1979).
93. Strutt, P.K., Gilbert, D.A., Novotny, H., Kim, Y.W.: Heat treatment of laser melted M2 tool set. In: Ferris, S.D., Leamy, H.J., Poate, J.M. (eds.): Laser-solid interaction and laser processing 1978. AIP Conference Proceedings, no. 50. American Institute of Physics, New York, pp. 232–238 (1979).
94. Duley, W.W.: Laser processing and analysis of materials. Plenum, New York (1983).
95. Tsao, J.Y., Aziz, M.J., Thompson, M.O., Peercy, P.S.: Asymmetric melting and freezing kinetics in silicon. Phys. Rev. Lett. 56: 2712–2715 (1986).
96. Kana, R.U. (ed.): Physical metallurgy. Haasena Metallurgy, Moscow (1983).
97. Chalmers, B.: Theory of crystallization. Mir, Moscow (1969).
98. Mullins, W.W., Sekerka, R.F.: Stability of a planar interfaces during solidification of a dilute binary alloy. J. Appl. Phys. 35: 444–451 (1964).
99. Coriell, S.R., Sekerka, R.F.: The effect of the anisotropy of surface tension and interface kinetics on morfological stability. J. Crystal Growth 34: 157–163 (1976).
100. Lyubov, B.Ya.: Crystallization theory in large volume. Nauka, Moscow (1975).
101. Willnecker, R., Herlach, D.M., Feuerbacher, B.: Evidence of nonequilibrium processes in rapid solidification of undercooled metals. Phys. Rev. Lett. 62: 2707–2710 (1989).
102. Colligan, G.A., Bayles, B.J.: Crystal growth of metastable phases. Acta Metall. 10: 895–899 (1962).
103. MacDonald, C.A., Malvezzi, A.M., Spaepen, F.: Picosecond time- resolved measurements of crystallization in noble metals. J. Appl. Phys. 65: 129–136 (1989).
104. White, C.W., Narayan, J., Joung, R.T.: Laser annealing of ion implanted silicon. In: Ferris, S.D., Leamy, H.J., Poate, J.M. (eds.): Laser-solid interaction and laser processing—1978. AIP Conference Proceedings no. 50. American Institute of Physics, New York, pp. 275–290 (1979).
105. Jackson, K.A., Leamy, H.J.: A comment on the solubility of impurities in laser annealed silicon. In: Ferris, S.D., Leamy, H.J., Poate, J.M. (eds.): Laser-solid interaction and laser processing—1978. AIP Conference Proceedings no. 50. American Institute of Physics, New York, pp. 102–107 (1979).
106. Baker, J.C., Cahn, J.W.: Thermodynamics of solidification. Acta Metall. 17: 575–578 (1969).
107. Aziz, M.J.: Model for solute redistribution during rapid solidification. J. Appl. Phys. 53: 1158–1168 (1982).
108. Mazumder, J., Kar, A.: Nonequilibrium processing with lasers. World Lasers 1: 17–24 (1988).
109. Astapchik, S.A., Tsarev, G.L., Beresa, N.A., Chebot'ko, I.S.: Sinergetic model of high-speed crystal growth from Al alloys. Vestsi Akad. Navuk B.S.S.R, Ser. Fiz. Tekh. Navuk 2: 13–18 (1987).
110. Derliglasova, I.F., Mulchenko, B.F., Roitenburg, E.I., Vorobijev, S.S., Metelkin, V.F.: Hardening method of Al alloys details. Patent from 22. 09. 1985.
111. Bogolubova, I.V., Deriglasova, I.F., Mulchenko, B.F.: Laser surface alloying of alloy AL 25. Metalloved. Term. Obrab: 24–25 (1988).
112. Deriglasova, I.F., Mulchenko, B.F., Vorobijev, S.S., Bogolubova, I.V., Sokolov, A.M.: Laser hardening of Al piston groove. Avtomob. Prom. 9: 25 (1987).
113. Afanasiev, Yu.V., Krokhin, Yu.N.: Gas dynamics theory of laser radiation influence to condensed media. T. Fiz. Inst. Akad. Nauk S.S.S.R. 52: 118–176 (1970).
114. Crout, B.P.: An application of kinetic theory to the problem of evaporation and sublimation of mono atomic gases. J. Math. Phys. 15: 1–54 (1936).
115. Romanov, G.S., Pustovalov, V.K.: Substance scattering from intensive evaporating metal surface. Izv. Akad. Nauk. S.S.S.R. Ser. Fiz. Mat. Nauk. 4: 84–95 (1967).
116. Anisimov, S.I.: About evaporation of the metal absorbing laser radiation. Sov. Phys. JETP 54: 339–342 (1968).

117. Moizhes, B.Ya., Nemchinsky, V.A.: Jet formation during evaporation to vacuum. Sov. Phys. Tech. Phys. 52: 684–689 (1982).
118. Samokhin, A.A.: About hydrodynamics scattering near evaporation front. Krat. Soobshch. Fizike Fiz. Inst. Akad. Nauk S.S.S.R. 6: 3–6 (1982).
119. Labuntsov, D.A., Krutov, A.P.: Analysis of intensive evaporation and condensation. Int. J. Heat Mass Transfer 22: 989–1001 (1979).
120. Mazhukin, V.I., Samokhin, A.A.: Some features of mathematical model for intensive surface evaporation. Dokl. Akad. Nauk S.S.S.R. 985: 830–833 (1985).
121. Mazhukin, V.I., Samokhin, A.A.: Phase transition kinetics under laser evaporation. Sov. J. Quant. Elec. 12: 2432–2437 (1984).
122. Mazhukin, V.I., Samokhin, A.A.: Radiation-induced vaporization kinetics from a surfaces into vacuum. Preprint Lebedev Phys. Inst. U.S.S.R. Acad. Sci. No. 170 (1984).
123. Knight, C.J.: Transit vaporization from a surface into vacuum. AIAA J. 20: 950–954 (1982).
124. Mazhukin, V.I., Pestryakova, G.A.: Mathematical modeling of processes of laser-induced surface evaporation. Dokl. Akad. Nauk S.S.S.R. 278: 843–847 (1984).
125. Mazhukin, V.I., Pestryakova, G.A.: Numerical analysis of erosion laser plasma influence on surface evaporation process. Izv. Akad. Nauk S.S.S.R. Ser. Fiz. 49: 783–790 (1985).
126. Mazhukin, V.I.: Kinetics of laser-induces surface evaporation of metal. In: Rykalin, N.N. (ed.): Concentrated energy flows influence on materials. Nauka, Moscow, pp. 182–199 (1985.).
127. Rykalin, N.N., Uglov, A.A., Nizametdinov, M.M.: Features of modeling of laser-solid interaction under high pressure environment. Sov. Phys. JETP 69: 722–726 (1975).
128. Galiev, A.L., Krapivin, L.I., Mirkin, L.I., Uglov, A.A.: Titan nitrid synthesis in nitrogen gas under high pressure and laser radiation. Dokl. Akad. Nauk S.S.S.R. 251: 336–340 (1980).
129. Rykalin, N.N., Uglov, A.A.: Laser-plasma metal treatment under high pressure of gases. Sov. J. Quant. Elec. 8: 1193–1197 (1981).
130. Pirri, A.N., Schlier, R., Northam, D.: Momentum transfer and plasma formation above a surface with a high-power CO_2-laser. Appl. Phys. Lett. 21: 79–81 (1972).
131. Barchukov, A.I., Bunkin, F.V., Konov, V.I., Prokhorov, A.M.: Investigation of gas low level breakdown near solid target under CO_2-laser radiation. Sov. Phys. JETP 66: 965–968 (1974).
132. Wei, P.S., Hall, R.B.: Emission spectra of laser-supported detonation waves. J. Appl. Phys. 44: 2311–2320 (1973).
133. Walters, C.T., Barmes, R.H., Beverly, R.E.: III. Initiation of laser-supported-detonation (LSD) waves. J. Appl. Phys. 49: 2937–2939 (1978).
134. Weyl, G., Pirri, A., Root, R.: Laser ignition of plasma of aluminum surfaces. AIAA J. 19: 460–469 (1981).
135. Leontovich, M.A., Kadomtsev, B.B. (eds.): Plasma theory problems. Energoizdat, Moscow (1982).
136. Gusev, I.V., Mazhukin, V.I.: Mathematical modeling of optical breakdown kinetics in aluminum vapors. Preprint Keldysh Inst. Acad. Sci. U.S.S.R. no. 22 (1990).
137. Stamm, M.R., Niesen, P.E.: Sensitivity of laser absorption wave formation to nonequilibrium and transport phenomena. AIAA J. 13: 205–208 (1975).
138. Mazhukin, V.I., Uglov, A.A., Chetverushkin, B.N.: Numerical investigation of a problem of dense gas laser-induced breakdown. Zhurn. Vychisl. Mat. Mat. Fiz. 20: 451–456 (1980).
139. Mazhukin, V.I.: Numerical modeling of dense molecular gas breakdown under influence of laser radiation focused on metal surface. Preprint Keldysh Inst. Acad. Sci. U.S.S.R. no 30 (1979).
140. Mazhukin, V.I., Uglov, A.A., Chetverushkin, B.N.: Molecular nitrogen optical breakdown in wide range of pressure near solid target. Sov. J. Quant. Elec. 9: 907–917 (1982).
141. Mazhukin, V.I., Uglov, A.A., Chetverushkin, B.N.: Low temperature laser plasma evolution in high pressure nitrogen medium. Dokl. Akad. Nauk S.S.S.R. 257: 584–589 (1981).
142. Mazhukin, V.I., Uglov, A.A., Chetverushkin, B.N.: Low temperature laser plasma near metal surfaces in high pressure gases (Review). Sov. J. Quant. Elec. 10: 679–701 (1983).
143. Mazhukin, V.I., Uglov, A.A.: Laser plasma near metal surface in high pressure gases. In: Paton, B.E. (eds.): Physics and chemistry of plasma metallurgical processes. Nauka, Moscow, pp. 135–159 (1985).
144. Mazhukin, V.I., Rykalin, N.N., Uglov, A.A., Chetverushkin, B.N.: Technique of gas nitrating of metal parts. Patent no. 1034428 (1982).
145. Mashukin, V.I., Semmler, U., Breslavskij, P.V., Takoeva, L.Yu.: Mathematische Modellierung des Laserschmelzens und -verdampfens homogener Materialien. Technische Universität Chemnitz Preprint no. 208 (1991).

146. Mashukin, V.I., Semmler, U., Breslavskij, P.V., Takoeva, L.Yu.: Das Programmpaket LASTEC-1 zur numerischen Simulation von Lasermaterialbearbeitungsprozessen. Technische Universität Chemnitz Preprint no. 209 (1991).

Authors' addresses: Acad. A. Samarskii and Dr. V.I. Mazhukin, Center for Mathematical Modeling, Russian Academy of Science, 4 Miusskaya Square, 125047 Moscow, Russia.

Verleger: Springer-Verlag KG, Sachsenplatz 4-6, A-1201 Wien, – Herausgeber: Prof. Dipl.-Ing. Dr. H. Engl, Institut für Mathematik, Johannes Kepler Universität Linz, A-4040 Linz. – Redaktion: Altenbergerstraße 69, A-4040 Linz. – Hersteller: Satz und Umbruch: Macmillan India Ltd., Bangalore-25. Offsetdruck: Novographic, Ing. W. Schmid, Maurer Lange Gasse 64, A-1238 Wien. – Verlagsort: Wien. – Herstellungsort: Wien. – Printed in Austria.